Quaternary Science Reviews 274 (2021) 107245

Contents lists available at ScienceDirect

Quaternary Science Reviews

journal homepage: www.elsevier.com/locate/quascirev

Nonlinear time series analysis of palaeoclimate proxy records

Norbert Marwan [a, b, *], Jonathan F. Donges [a, c], Reik V. Donner [a, d], Deniz Eroglu [e]

[a] Potsdam Institute for Climate Impact Research (PIK), Member of the Leibniz Association, Telegrafenberg A31, 14473, Potsdam, Germany
[b] Institute of Geosciences, University of Potsdam, Karl-Liebknecht-Straße 24-25, 14476, Potsdam-Golm, Germany
[c] Stockholm Resilience Centre, Stockholm University, Kräftriket 2B, 11419, Stockholm, Sweden
[d] Department of Water, Environment, Construction and Safety, Magdeburg-Stendal University of Applied Sciences, Breitscheidstraße 2, 39114, Magdeburg, Germany
[e] Faculty of Engineering and Natural Sciences, Kadir Has University, 34083, Istanbul, Turkey

ARTICLE INFO

Article history:
Received 9 September 2021
Accepted 6 October 2021
Available online 11 November 2021

Handling editor: Martin Trauth

Keywords:
Nonlinear time series analysis
Palaeoclimate proxy
Pliocene
Pleistocene
Climate transition
Regime shift

ABSTRACT

Identifying and characterising dynamical regime shifts, critical transitions or potential tipping points in palaeoclimate time series is relevant for improving the understanding of often highly nonlinear Earth system dynamics. Beyond linear changes in time series properties such as mean, variance, or trend, these nonlinear regime shifts can manifest as changes in signal predictability, regularity, complexity, or higher-order stochastic properties such as multi-stability. In recent years, several classes of methods have been put forward to study these critical transitions in time series data that are based on concepts from nonlinear dynamics, complex systems science, information theory, and stochastic analysis. These include approaches such as phase space-based recurrence plots and recurrence networks, visibility graphs, order pattern-based entropies, and stochastic modelling. Here, we review and compare in detail several prominent methods from these fields by applying them to the same set of marine palaeoclimate proxy records of African climate variations during the past 5 million years. Applying these methods, we observe notable nonlinear transitions in palaeoclimate dynamics in these marine proxy records and discuss them in the context of important climate events and regimes such as phases of intensified Walker circulation, marine isotope stage M2, the onset of northern hemisphere glaciation and the mid-Pleistocene transition. We find that the studied approaches complement each other by allowing us to point out distinct aspects of dynamical regime shifts in palaeoclimate time series. We also detect significant correlations of these nonlinear regime shift indicators with variations of Earth's orbit, suggesting the latter as potential triggers of nonlinear transitions in palaeoclimate. Overall, the presented study underlines the potentials of nonlinear time series analysis approaches to provide complementary information on dynamical regime shifts in palaeoclimate and their driving processes that cannot be revealed by linear statistics or eyeball inspection of the data alone.

1. Introduction

Past climate conditions, variability, and transitions are essential to understand current and future climate changes. In particular, the Plio-Pleistocene can be used as an analogue of future greenhouse climate and how and which regime shifts in large-scale atmospheric and ocean circulation can be expected in a warming world (Burke et al., 2018; Steffen et al., 2018). Moreover, it has been a period of important steps in human evolution, where significant climate regime shifts have most likely influenced the evolution and the migration of human ancestors (deMenocal, 1995; Potts, 1996; DeMenocal, 2004; Trauth, 2005; Staubwasser and Weiss, 2006; Donges et al., 2011b). A better understanding of abrupt climate changes, the pattern of variations, long-distance interrelationships, feedback loops, or the type of dynamics can further help to build our picture of the world and improve corresponding modelling approaches.

The last decades have shown an increasing availability and progress of quantitative approaches in geosciences, ranging from provenance analysis, over rock magnetic measurements, X-ray fluorescence analysis, to isotope geochemistry. Such quantitative approaches have enriched the qualitative studies significantly and

* Corresponding author. Potsdam Institute for Climate Impact Research (PIK), Member of the Leibniz Association, Telegrafenberg A31, 14473, Potsdam, Germany.
E-mail address: marwan@pik-potsdam.de (N. Marwan).

https://doi.org/10.1016/j.quascirev.2021.107245

allowed new insights that would not have been able to get without them (Sauramo, 1918; Stanley, 1978; Haug and Tiedemann, 1998; Trauth et al., 2021). Most quantitative analysis is traditionally focusing on linear methods of statistics and time series analysis (such as correlations, power spectra, regression analysis, detection of breakpoints, etc.; Trauth (2021); Mudelsee and Stattegger (1997)) as well as partially on extensions thereof (e.g., time-frequency decomposition employing continuous wavelet transforms, Bayesian approaches to breakpoint detection and regression replacing classical maximum likelihood or least squares estimators (e.g. Schütz and Holschneider, 2011)). Such analyses provide important information on the levels displayed by certain proxy variables and, thus, allow tracing long-term changes of time-average environmental and climatic conditions. However, their application potential can be limited by the fact that real world systems usually consist of many interacting components with feedbacks and nonlinear interrelationships, behave in a more chaotic rather than periodic way, vary in a fashion that cannot be described by a normal distribution (Schölzel and Friederichs, 2008), exhibit distinct behaviours in terms of their extreme event statistics (Albeverio et al., 2006), or represent critical transitions to qualitatively different dynamical regimes (such as tipping points) (Lenton et al., 2008; Schellnhuber, 2009). Concepts from complex systems science, complex networks, and nonlinear dynamics are more appropriate for such problems (Boers et al., 2021; Fan et al., 2021). In the light of the critical impacts of climate and environmental changes on human societies, quantitative investigations of large-scale regime shifts (Rocha et al., 2018; Boers and Rypdal, 2021), early warning indicators of such shifts (Dakos et al., 2008; Scheffer et al., 2009; Boettner et al., 2021), and short-term ecosystem responses (Scheffer and Carpenter, 2003; Prasad et al., 2020) on the base of palaeoclimate archives are required. Such insights on critical regime shifts and other large-scale nonlinear changes in Earth system dynamics are highly relevant for determining planetary boundaries delineating a safe operating space that allows for sustainable development of human societies in the Anthropocene (Rockström et al., 2009; Hughes et al., 2013; Steffen et al., 2015).

In this study, we review and discuss a selection of data analysis methods that have been widely applied to study complex systems and have their origin in nonlinear dynamics, stochastic modelling, and information theory to identify regime shifts of the palaeoclimate dynamics. While there are many more methods of nonlinear data analysis or machine learning that could be applied in principle, we focus here only on a selection that might be of particular interest for the palaeoclimate researcher when studying regime transitions. After a brief look at linear methods, we will first introduce concepts of nonlinear methods before demonstrating their abilities on marine palaeoclimate records that represent the Plio-Pleistocene climate variation on the northern African continent.

2. Methods

A plethora of quantitative methods to study palaeoclimate processes have been developed and are available for different purposes. This includes linear and nonlinear methods, or methods using frequentist and Bayesian inference. The selection of the appropriate method depends, of course, on the specific research question.

Transitions in climate records can occur at different levels. Related to the time scale, the signal can change abruptly, such as the global temperature after an asteroid impact (Brugger et al., 2017), or gradually, such as the slower glaciation (compared to the abrupt warming during the interstadials) during the stadials of the glaciation (Dansgaard et al., 1993). We can consider changes of the statistical moments of the time series, such as a change in the mean value (e.g., changing global temperature; Westerhold et al. (2020)) and the variance, or even in higher moments (e.g., skewness of the amplitude distribution). Gradual changes of the signal's mean correspond to trends and are commonly studied by ramp fit models (Mudelsee and Schulz, 1997). More subtle changes in the underlying dynamics can be even more interesting, because they are usually not so obviously visible in the time series, like a change in the mean or variance. For example, the period of a cyclical climate variation can change, as it was found for the mid-Pleistocene transition (MPT) with a shift from a 41 ka to 100 ka climate cycle (Clark et al., 2006). With respect to tipping points, the autocorrelation within the signal can be of additional benefit, indicating early warnings of critical climate transitions (such as during the Cenozoic climate (Boettner et al., 2021)). When considering the climate as a dynamical system, it might also be of interest to determine the dimension of the system (i.e., how many differential equations would be necessary to describe the observed dynamics) or whether the system's dynamics can be characterised as a stochastic, periodic, or chaotic process. Albeit the latter type of behavior corresponds to a deterministic process (which means that its states can be computed), it is difficult to predict.

Transitions in climate records based on changes of first statistical moments, trends or periodicity can be analysed with linear methods. For example, to statistically identify transitions of mean and variance, a running Mann-Whitney or Ansari-Bradley test can be used (Trauth et al., 2009). Regression-based models (Mudelsee and Schulz, 1997) and Bayesian change point detection (Schütz and Holschneider, 2011) are further suitable tools for this research question. Changes in the cyclicities can be analysed with evolutionary power spectra (Trauth, 2021) or with wavelet analysis (Lisiecki, 2010). Further developments consider decompositions of the palaeoclimate time series using wavelet transform or singular spectrum analysis (Vautard and Ghil, 1989; Ghil, 2002).

Following the progress in nonlinear dynamics and complexity science in the 1970s and 1980s, additional and novel concepts have found their way into Earth sciences. Fractal dimensions and Lyapunov exponents have been promising ideas to better understand, model, and predict the climate system. However, after a first euphoria, it became clear that palaeoclimate data, in particular, comes with problems that make it almost impossible to apply such methods reliably (Grassberger, 1986; Maasch, 1989; Schulz et al., 1994): the data is non-stationary, the sampling is irregular, the uncertainties are too high due to dating uncertainties, many degree of freedom, and bad signal-to-noise ratio. Despite the problems with some methods, other methods were more successful, such as the already mentioned singular spectrum analysis (Vautard and Ghil, 1989), potential analysis (Livina et al., 2010), or recurrence analysis (Marwan et al., 2007). In the following, we will focus on selected methods based on concepts of complex systems and nonlinear dynamics that can be used to study different aspects of transitions in palaeoclimate dynamics (see Table 1). We will also add information about available software packages. The corresponding links to the software can be found in the Sect. 7, Table 4.

2.1. Windowing approach

The detection of transitions in the dynamics is based on the idea that some statistical properties change with time. To evaluate such changes, we have to calculate a certain quantity or measure at a certain point in time and compare it with previous or later values of this quantity. Most of the quantities need, however, a larger number of values to be calculated, i.e., we need to divide our time series into short pieces or time windows of length w. Such a time window

Table 1
Overview on the methods of nonlinear time series analysis discussed and partly compared for applications to Plio-Pleistocene palaeoclimate variability in this study.

Type	Method	Focus	References
Stochastic modeling	potential analysis	multi stability of underlying processes	Kwasniok and Lohmann (2009); Livina et al. (2010); Kwasniok and Lohmann (2012)
Statistical mechanics and information theory	entropies, order patterns	Time series complexity	Bandt and Pompe (2002); Balasis et al. (2013); Zanin and Olivares (2021)
Phase-space based approaches	recurrence plots, recurrence networks	time series classification, dynamical transitions	Marwan et al. (2007); Boers et al. (2021); Zou et al. (2019)
Visibility relationships	time-directed visibility graphs	temporal reversibility	Lacasa et al. (2012); Donges et al. (2013)

is then moved over the entire time series. The window has a starting point t_1, an endpoint t_2, and a center point $(t_2 - t_1)/2$. The quantity calculated within this window is then assigned to this centre point and, thus, provides a new time series of this quantity. The moving step of this window *ws* sets the temporal resolution of the new quantity time series. However, the smaller *ws*, the larger the overlap and the more redundant the information of subsequent quantity values. We have, therefore, to find a good trade-off between redundant information and temporal resolution. A change of this quantity over time can then be interpreted concerning the investigated regime transition. Moreover, we have to consider the window size when interpreting the results. For example, using a time window of length 410 ka, an abrupt increase of a transition measure at 2 Ma before present (BP) would mean that the transition happened not earlier than approximately 1.795 Ma BP (because of the used centre point of the window). A single point covers a period of 410 ka; for a used offset of 41 ka, two consecutive points of time correspond to 410 + 41 ka, and so on.

2.2. Statistical mechanics and information theory

Complexity is a concept that characterizes the dynamical behaviour of a given complex system whose many parts interact in many different ways. Complex behaviour (and chaotic dynamics) usually appear in nonlinear systems and can be measured with various complexity measures. One of the most well-known complexity measures is the entropy (a measure of information theory), which measures the uncertainty in a system (Shannon, 1948). The entropy measure has been used to detect abrupt changes and regime transitions from data in different disciplines such as life sciences, engineering, economics, and Earth sciences (Gapelyuk et al., 2010; Li et al., 2013; Afsar et al., 2016; Zhao et al., 2020).

Shannon entropy. For a given time series $x(t)$, the Shannon entropy S is defined as

$$S = -\sum_x \rho(x) \log \rho(x), \tag{1}$$

where $\rho(x)$ is the probability density function (PDF) of the values x of the time series (in practice, this is approximated by n discrete bins i, with h_i the probability that the time series value x falls within the interval i and $S = -\sum_i^n h_i \log h_i$). The PDF is a function that specifies the probability of a randomly picked point from the observation $x(t)$ existing within a particular interval (range of values). As an intuitive point of view, if the probabilities are approximately the same for each specified interval (i.e., when having a homogenous probability distribution), the entropy is expected to be high since the randomly picked point can be in one of the intervals with equal probability. In other words, there is no way to find an interval in which a randomly chosen number would be with high probability. Contrarily, if the distribution is heterogeneous, then the entropy is expected to be low and we will be much less uncertain in predicting a random pick from the data (Fig. 1). Hence, the Shannon entropy defined solely on individual time series data is a purely distributional property. Nevertheless, a change of the entropy over time can be used to identify exceptional states, an application that is used, e.g., to detect intense magnetic storms (Balasis et al., 2008).

Simple PDF dependent statistical measures like Shannon entropy do not consider the order of samplings, i.e., they neglect deterministic changes in the data. Therefore, we have to be careful in interpreting the Shannon entropy value calculated directly from the data with respect to the complexity of the dynamics (Fig. 2).

In order to incorporate different aspects of the data, such as the dynamics, various concepts and approaches have been developed for the construction of a suitable PDF. These different procedures led to various entropy measures such as the Tsallis entropy, order (permutation) entropy, and block entropy (Balasis et al., 2013; Boaretto et al., 2021). Further and more advanced information based measures, derived from the dynamical systems theory, are, e.g., Kolmogorov-Sinai entropy or correlation entropy (Grassberger and Procaccia, 1984).

Order Entropy (Permutation Entropy). As mentioned above, changing the order of the numbers in a time series does not change the value of the Shannon entropy. Dynamically different systems can have very similar PDFs and, therefore, similar entropy values due to order ignorance (Fig. 2).

To take into account the dynamics of the system, short sequences of the time series have to be considered. A simple approach for such is to consider the local rank order of subsequent values of the time series (Zanin and Olivares, 2021). Such order pattern reduces the value range to only a few numbers and encodes the dynamical behaviour. For calculating the entropy, the PDF of the order patterns is used.

In the simplest case (pattern of order two, $d = 2$), a time series $(x_1, x_2, \ldots, x_N)$ can be discretized by comparing the values at two time points

$$\pi_i = \begin{cases} 0 & x_i < x_{i+\tau}, \\ 1 & x_i > x_{i+\tau}, \end{cases} \tag{2}$$

where τ is a delay parameter that allows some adjustment to a time scale of interest (such as the typical period of a cyclic signal). In the present study, we use order patterns of degree $d = 3$, providing six different order patterns (Fig. 3). A degree of $d = 3$ is usually sufficient to describe the important dynamical properties of the time series (Bandt and Shiha, 2007). Moreover, the number of possible order patterns is $d!$ In order to estimate a reliable PDF of the $d!$ different order patterns, we need longer and longer time series for larger d, which are often not available in real applications.

Then, the order (or permutation) entropy is the Shannon entropy of the PDF of the order patterns

$$S_{\text{order}} = -\sum_{i=1}^{d!} \rho(\pi_i) \log \rho(\pi_i). \tag{3}$$

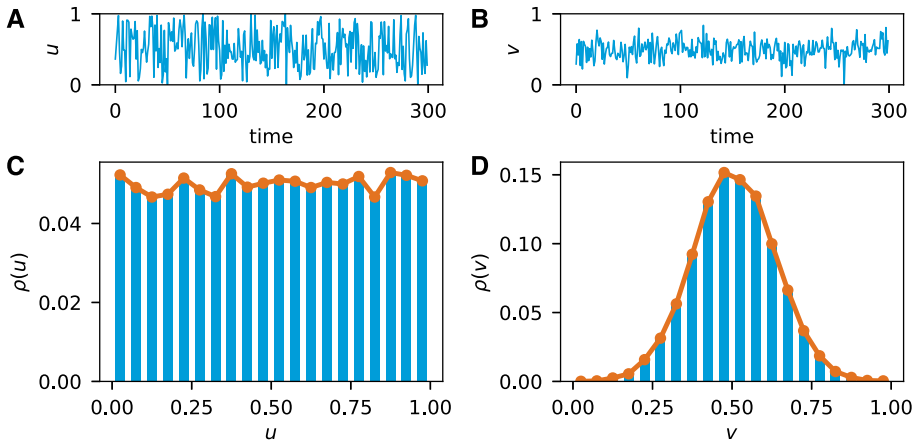

Fig. 1. Illustration of (A, B) random time series u and v and (C, D) their probability density functions $\rho(u)$ and $\rho(v)$. The entropy of (A, C) u with uniform distribution is $S_u \approx 3.0$ and (B, D) v with normal distribution is $S_v \approx 2.37$.

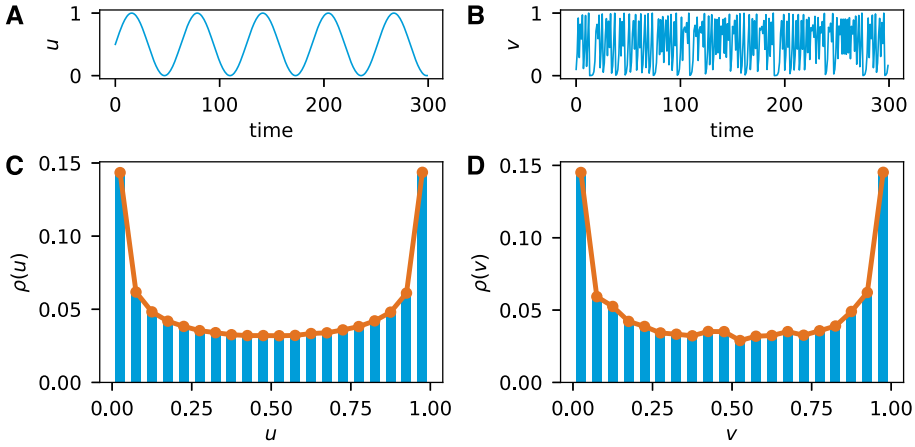

Fig. 2. Entropy measures can fail detecting different dynamical regimes, as such of (A) a sinusoidal wave u and (B) a chaotic signal (generated using logistic map $v(t+1) = 4v(t)(1 - v(t))$). Although the dynamics represented by u and v is entirely different, the (C, D) PDFs are similar. Therefore, the entropy of u and v are $S_u \approx S_v \approx 2.84$.

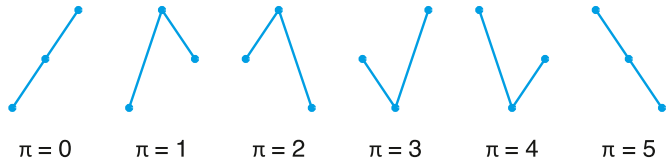

Fig. 3. Order patterns of dimension $d = 3$.

Such entropy measure enables us to detect different dynamical regimes (Boaretto et al., 2021), because some dynamics is related to a tendency to certain order patterns (e.g., periodic dynamics), where others can lead to more equally frequent order patterns (e.g., stochastic dynamics; Fig. 4). Because it does not characterize the PDF of the amplitude distribution, processes with the same dynamics but different PDF cannot be distinguished (Fig. 5). Thus, the use of the Shannon entropy and the order entropy depends on the research question, i.e., whether we need to characterize the amplitude distribution or the dynamics.

Order entropy can be a useful measure to check anomalies in the data or to identify such segments that are not associated with the climatic processes of interest (Garland et al., 2018). It has also be used to detect periodic changes in climate proxies of the late Silurian and to establish a corresponding astrochronology (Spiridonov et al., 2020).

Confidence intervals. Applying the windowing approach, the entropy measures are changing over time. We might ask, how significant such variation is. To assess the significance, we consider a null-hypothesis of "no temporal change" in the considered characteristic of the time series, given the properties of this time series. Unfortunately, for nonlinear data analysis, no general significance test is available with tables and significance values in textbooks. Therefore, we have to create the test individually, incorporating the specific settings and conditions given by the research question. To test the above null-hypothesis, we use the original time series to create artificial time series which comply with the specific null-hypothesis. Such time series are also called surrogates. We can create such surrogate time series by bootstrapping values from the original time series. The entropy measure is then calculated from the surrogate. By repeating this procedure many times, we get an empirical test distribution of the entropy measure, which represents the entropy values to be expected under the null-hypothesis. Now, we can use the 5% and 95%-quantiles of this test distribution to define a two-sided 90%-confidence interval. If the entropy measure in a certain window exceeds the confidence interval, we consider this value as significantly different and the dynamics has changed.

Software. Entropy can be easily calculated from time series by

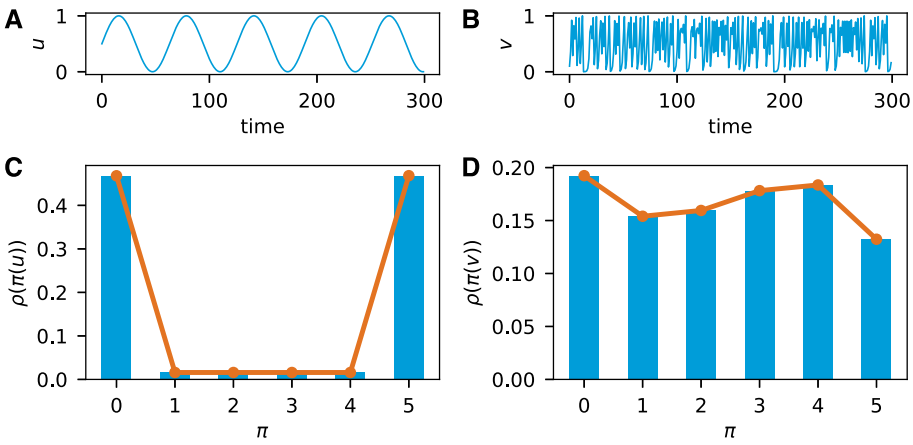

Fig. 4. In contrast to the Shannon entropy, the order (permutation) entropy ($d = 3$) detects different dynamical regimes, such as (A) a sinusoidal signal u and (B) a chaotic signal (generated using logistic map $v(t+1) = 4v(t)(1 - v(t))$). Although the PDF of time series are similar (see Fig. 2), the PDF of order patterns differ from each other (C, D) and the order entropy of u and v differs clearly, $S_{\text{order}}(u) \approx 0.98$ and $S_{\text{order}}(v) \approx 1.78$.

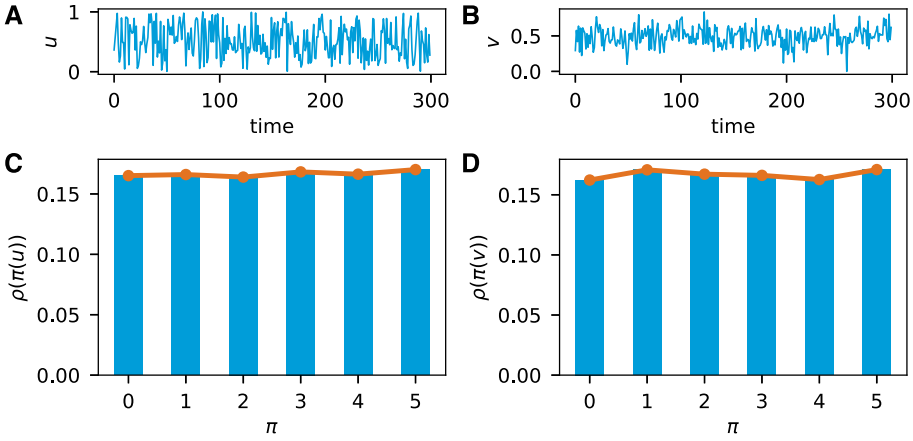

Fig. 5. Illustration of (A, B) white noise u and v with different PDFs $\rho(u)$ and $\rho(v)$, but similar PDFs of the order patterns (C, D). The order entropy does not distinguish between these two random processes: $S_u \approx 1.79$ and $S_v \approx 1.79$.

their probability distributions. This measure is often part in larger software solutions, such as in the *CRP Toolbox* for MATLAB (Sect. 7, Table 4). For order entropy, specific packages are available, e.g., for Python the *ordpy* package (Pessa and Ribeiro, 2021), or for MATLAB the *Permutation entropy* package.

2.3. Stochastic modelling (potential analysis)

The behaviour of many dynamical systems can be described by a stochastic differential equation, e.g., a changing climate which is forced by a stochastic process. The conceptual model for such a process can be described by the simple equation (which is a stochastic differential equation) (Gardiner, 2009; Kwasniok and Lohmann, 2009, 2012)

$$\frac{dx}{dt} = -\frac{dU(x)}{dx} + \sigma dW, \tag{4}$$

with x corresponding to the slowly changing climate state, $U(x)$ the potential which restricts the possible states x, σ the amplitude of the stochastic process, and W a real valued continuous time stochastic (Wiener) process. The complexity of the potential $U(x)$ determines the number of states, e.g., for a double-well potential $U(x) = -2x^2 + x^4$ we will find two different states between which

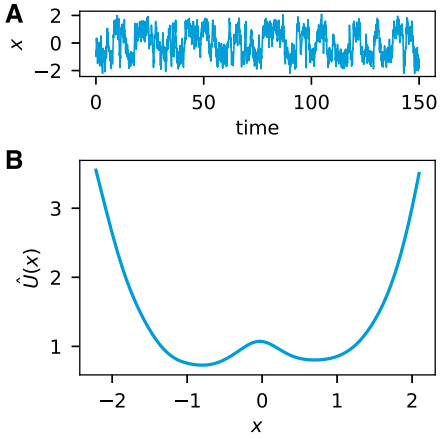

Fig. 6. A stochastic process simulated using Eq. (6) with the double-well potential $U(x) = -2x^2 + x^4$. Using the generated random time series x, the potential function $\hat{U}(x)$ is reconstructed. As the double-well potential is considered in the time series generation, we find two wells ($n_U = 2$) in the reconstructed potential function.

the system can jump (Fig. 6A).

By exploiting the associated Fokker-Planck equation, we can find the probability density function of the process depending on the potential (Risken, 1989):

$$\rho(x) \sim \mathrm{e}^{-\frac{2U(x)}{\sigma^2}}. \tag{5}$$

The PDF $\rho(x)$ can be estimated from a time series x using a standard Gaussian kernel estimator (Silverman, 1986). Thus, we can now find a reconstruction of the potential by (Fig. 6)

$$\hat{U} = -\frac{\sigma^2}{2}\log \rho(x). \tag{6}$$

The parameters of Eq. (4) can also be estimated by more sophisticated approaches, such as the Kramers-Moyal or Mori-Zwanzig approaches (Friedrich et al., 2011; Hassanibesheli et al., 2020) or the unscented Kalman filter (Kwasniok and Lohmann, 2009, 2012), which have been mainly applied to trace dynamical regime changes (e.g., DO events) in ice core data. However, for the sake of simplicity, we use here the simple approach using the PDF estimation.

Counting the wells of the reconstructed potential $\hat{U}$, we have an estimate of the number of possible states n_U (Livina et al., 2010). This approach was successfully applied to study the bifurcation behaviour of the climate in the Pliocene using benthic stable isotope and ice core data (Livina et al., 2010, 2011, 2012).

Software. For the simple approach of kernel based PDF estimation as used here, the corresponding functionality is usually already included in many software packages (e.g., in *scipy* for Python or in the *Statistics and Machine Learning Toolbox* for MATLAB). Parameter estimation using the Kramers-Moyal approach or the unscented Kalman filter can be performed using the *kramersmoyal* and *FilterPy* packages for Python.

2.4. Phase space-based approaches

Dynamical systems theory considers the underlying dynamics of the observed, measured system. The idea is that all n state variables of the dynamical system span an n-dimensional space and that a point in such a space corresponds to the state of the system (Fig. 7B). With time, such a point moves in this phase space and forms a trajectory (the phase space trajectory). Such a phase space trajectory is the starting point for different analysis approaches, in particular for many nonlinear measures.

Phase space reconstruction. In many practical situations, only one observable (i.e., a single time series) is available and the phase space has to be reconstructed (Takens, 1981). Several approaches have been suggested for phase space reconstruction, using time shifted copies or derivatives (Lekscha and Donner, 2018; Kraemer et al., 2021). For the sake of simplicity, here we use the widely used approach of time-delay embedding with constant delays (Packard et al., 1980), where the phase space vector $\vec{x}(t) = \vec{x}_i$ (with $t = i\Delta t$ and Δt the sampling time) is formed from one observation $x(t)$ by time-shifted copies

$$\vec{x}_i = \left(x_i, x_{i+\tau}, \ldots, x_{i+(m-1)\tau}\right),$$

with m and τ the embedding dimension and the embedding delay (Figs. 7 and 8B). Under general conditions, the reconstructed phase space can be considered topologically equivalent to the original phase space. The embedding delay τ has to be chosen in such a way, that a dependence between the vector components of $\vec{x}$ vanishes. An often used means of determining the delay is the *autocorrelation function* $C(\tau) = \langle x_i\, x_{i-\tau}\rangle$ ($\langle x\rangle = 0$, $\sigma(x) = 1$, and $\langle\bullet\rangle$ denoting the arithmetic mean). A delay may be appropriate when the autocorrelation approaches zero for this value of delay or at least falls below a certain de-correlation threshold (corresponding to the autocorrelation time τ_c, which is where $C(\tau_c) \approx 1/\mathrm{e}$) (Kantz and Schreiber, 1997), minimizing the linear correlation between the components (absence of linear correlation does not mean necessarily statistical independence in general, but only linear independence).

A practically efficient and widely used approach for the determination of the smallest sufficient embedding dimension m uses the number of *false nearest neighbours*. The basic idea is that by decreasing the embedding dimension an increasing amount of phase space points will be projected into the neighbourhood of any phase space point, even if they are not real neighbours. Such points are called *false nearest neighbours* (FNNs). The simplest method uses the amount of these FNNs as a function of the embedding dimension in order to find the minimal embedding dimension (Kantz and Schreiber, 1997). Such a dimension has to be taken where the FNNs vanish. Additional criteria could be applied, e.g., the ratios of the distances between the same neighbouring points for different dimensions (Kennel et al., 1992; Cao, 1997; Kraemer et al., 2021).

Phase space properties. A classical approach of analyzing the phase space is the estimation of the correlation dimension and general fractal dimensions (Grassberger and Procaccia, 1983). Whereas the integer part of the dimension can give some hint on the degree of freedom of the dynamical system (i.e., how many variables we would need to describe such a dynamics), a possible fractional part of the dimension value is considered to be of special interest, because it means that the phase space trajectory has fractal properties and the dynamics is rather irregular. However,

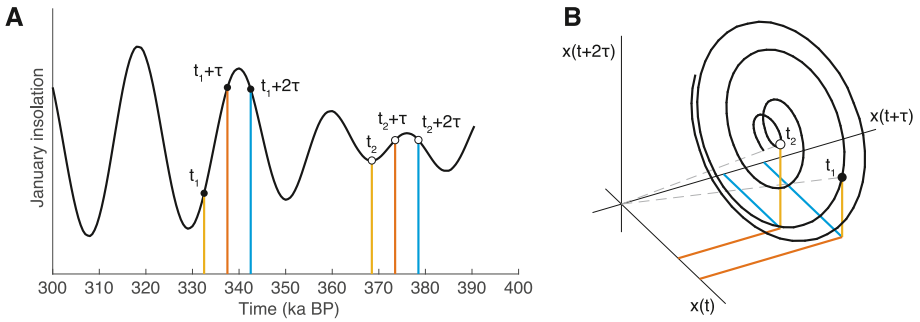

Fig. 7. Illustration of the phase space reconstruction of (A) a time series (January insolation at latitude 20°N) by time-delay embedding (B). A state at time t_1 is constructed from time series values that are shifted by a small delay τ (black points in A) which serve as the coordinates in the phase space (B). Black points correspond to time t_1 and white points to time t_2.

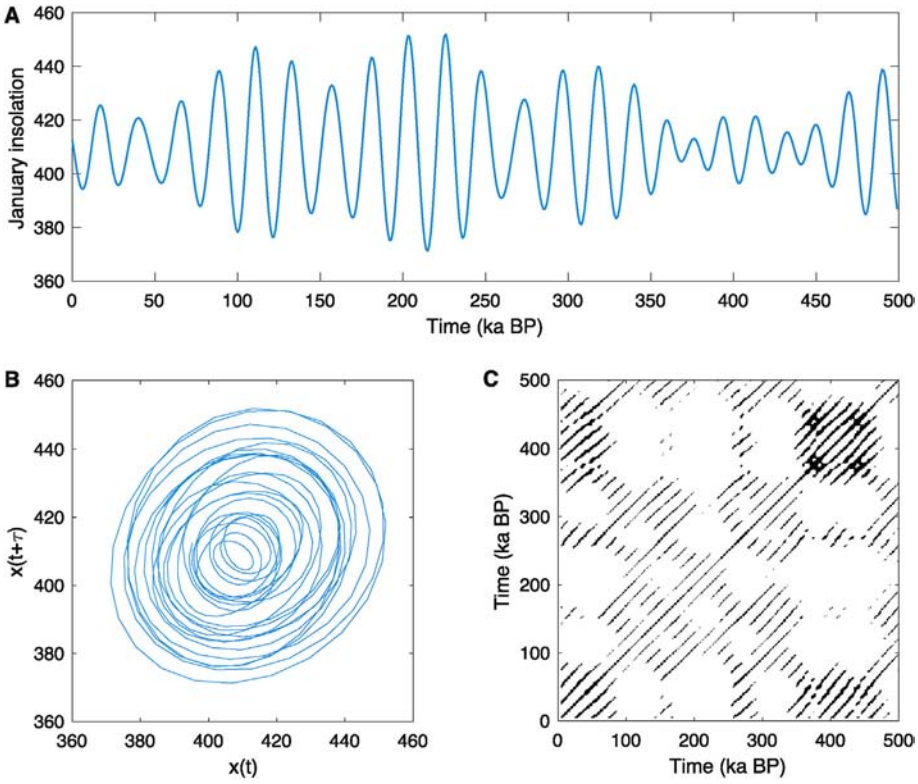

Fig. 8. (A) January insolation at latitude 20°N for the last 500 ka as an exemplary time series to illustrate the phase space and recurrence plot approach. (B) Phase space representation of the insolation time series in (A) based on a time delay embedding using a delay of $\tau = 6$ ka and embedding dimension $m = 2$. (C) Recurrence plot of the insolation time series; the recurrence threshold $\epsilon = 10$. The cyclical variations are visible by the periodic diagonal lines in the recurrence plot.

despite the initial euphoria and the estimations of the fractal dimension from numerous geophysical data sets, it finally turned out that this measure is often too sensitive to the amount of noise typical for this kind of data (Maasch, 1989; Schulz et al., 1994). Moreover, the initial requirement of long and stationary records can also not be sophisticated by the usually available data (Eckmann and Ruelle, 1992). Estimations of fractal dimensions from real world data have been, therefore, controversial (e.g., Grassberger, 1986; Möller et al., 1989; Gershenfeld, 1992).

Another fundamental property of interest of the phase space trajectory is its divergence behaviour. Tiny displacements in the phase space can result in heavily diverging trajectories, i.e., to completely different states. In such cases, we refer to this as a chaotic behaviour, because the states depend strongly on the initial conditions and are not predictable. The diverging of the trajectory due to small deviations in initial values is measured by the Lyapunov exponent (Wolf et al., 1985; Kantz, 1994). Positive values indicate chaotic dynamics. But similar to the estimation of fractal dimensions, a reliable estimation of the Lyapunov exponent requires also long time series (Eckmann and Ruelle, 1992). If only the largest Lyapunov exponent is of interest, several approximating approaches have been suggested (Kantz, 1994; Rosenstein et al., 1993).

Recurrence plots. A more recent approach of analyzing complex dynamics by the phase space trajectory is by investigating its recurrence behaviour. A powerful framework for recurrence analysis is provided by the recurrence plot (RP) (Marwan et al., 2007). A RP represents all such time points j at which a state $\vec{x}_i$ recurs:

$$R_{i,j} = \begin{cases} 1 & \text{if } \vec{x}_i \approx \vec{x}_j, \\ 0 & \text{otherwise.} \end{cases} \tag{7}$$

The recurrence of a state is usually defined by the closeness of two states, measured by comparing their spatial distance $D_{i,j} = \left\| \vec{x}_i - \vec{x}_j \right\|$ with a threshold ϵ:

$$R_{i,j} = \Theta(\epsilon - D_{i,j}), \tag{8}$$

with Θ the Heaviside function ($\Theta(x < 0) = 0, \Theta(x \geq 0) = 1$). Different research questions and applications can require different recurrence definitions (Marwan et al., 2007). Here we use one based on Euclidean norm and selecting a threshold ϵ to ensure a predefined recurrence point density, $RR = N^{-2} \sum_{ij} R_{i,j}$ (Kraemer et al., 2018). The resulting recurrence matrix $\mathbf{R}$ is a $N \times N$ binary matrix (with N the number of considered states, i.e., time points).

Recurrence quantification analysis. Although the RP is a visualization technique for recurrences in phase space, it is the base for different recurrence quantification approaches. By looking at a RP (Fig. 8C), we identify some characteristic features: lines that are parallel to the main diagonal and some vertically extended block structures (vertical lines). The presence of diagonal and vertical lines reflects the dynamics of the system and is related to divergence (Lyapunov exponents) and intermittency (Marwan et al., 2002, 2007; Thiel et al., 2004). Following a heuristic approach, a quantitative description of RPs based on these line structures was introduced and is known as recurrence quantification analysis (RQA) (Zbilut and Webber, Jr., 2007; Marwan, 2008) that has demonstrated its power and potential in numerous scientific disciplines for various applications. It can be used to study regime changes, dynamical transitions, characterizing dynamics, classifying different dynamical behaviour, detecting synchronization, and coupling directions (Marwan et al., 2007; Marwan, 2008; Webber, Jr. et al., 2009). For palaeoclimate research, it is a

promising tool to identify climate transitions, such as the Cenozoic climate regimes of hothouse, warmhouse, coolhouse, and cold-house states (Westerhold et al., 2020), Pleistocene and Holocene changes in the Asian monsoon system (Eroglu et al., 2016; Lechleitner et al., 2017; Goswami et al., 2018; Han et al., 2020) African climate (Trauth et al., 2021) and El Niño/Southern Oscillation activity (Marwan et al., 2003), Holocene vegetation patterns and environmental changes (Spiridonov et al., 2019, 2021), or decadal solar variations (Voss et al., 1996). It was also used to identify global temperature forcing in historical data (Goswami et al., 2013) and as a test framework in a study on the volcanic impact on the coupling between El Niño/Southern Oscillation and Indian Summer monsoon (Singh et al., 2020).

Epochs of the phase space trajectory that evolve in a similar way, i.e., run close and parallel in the phase space, cause diagonal structures in the RP. The length of such diagonal line structures depends on the predictability and, hence, the dynamics of the system (periodic, chaotic, stochastic). Therefore, the histogram $P(l)$ of diagonal line lengths l is one of the important features used by several RQA measures for characterizing the system's dynamics.

A central RQA measure is quantifying the fraction of recurrence points $R_{i,j} \equiv 1$ that form diagonal lines:

$$DET = \frac{\sum_{l=l_{\min}}^{N} l P(l)}{\sum_{l=1}^{N} l P(l)}. \tag{9}$$

This measure is called *determinism* because the relative amount of diagonal lines vanishes for stochastic, but is high for deterministic processes. We can use this measure as an indicator of predicability. Here, we use it in a relative manner, i.e., interpret dynamics of increased DET values as relatively more predictable than such with lower values. For the definition of a diagonal line, we use a minimal length $l_{\min}$ that should be of the order of the auto-correlation time (Marwan et al., 2007).

Another RQA measure is quantifying slowly changing states, as occurring during laminar phases (intermittency). Such dynamics result in vertical structures in the RP. Similar to the definition of DET, we can calculate the fraction of recurrence points forming vertical structures to all recurrence points,

$$LAM = \frac{\sum_{v=v_{\min}}^{N} v P(v)}{\sum_{v=1}^{N} v P(v)}, \tag{10}$$

which is called *laminarity* (Marwan et al., 2007). $P(v)$ is the histogram of vertical lines of length v. Measures based on vertical structures allow to detect chaos-chaos transitions, whereas measures based on diagonal lines detect chaos-order transitions. Here we use this measure to evaluate the persistence of variations relatively.

The confidence of the variations in the recurrence measures (using the moving windows approach) can be determined with a specific, bootstrap based statistical test (Marwan et al., 2013). For all moving windows s, the individual distributions of diagonal line lengths $P_s(l)$ are merged $P^*(l) = \sum_s P_s(l)$. From this distribution, line lengths are drawn and used to construct a new individual distribution $\hat{P}_s(l)$, from which we calculate the DET measure. This bootstrapping of line lengths is repeated many times, producing a distribution of DET values which correspond to an overall dynamics, i.e., representing a baseline dynamics. The 5% and 95%-quantiles of this empirical test distribution are then used as the 90%-confidence interval and to assess the significance of excursions of the DET values over time. A similar approach is used for the vertical line based measure LAM.

Recurrence networks. An extension to quantify the recurrences in phase space is to identify the recurrence matrix **R** as a link matrix **A** of a network and to use measures from complex network theory (Marwan et al., 2009; Donner et al., 2010). Excluding self-loops, we obtain **A** from the RP by removing the identity matrix,

$$A_{i,j} = R_{i,j} - \delta_{i,j}, \tag{11}$$

where $\delta_{i,j}$ is the Kronecker delta ($\delta_{i,j\neq i} = 0$, $\delta_{i,j=i} = 1$). The resulting unweighted and undirected network consists of phase space vectors (associated with their time points) as nodes and recurrences as links (see Fig. 9). A difference to the recurrence quantification analysis is that in a network the nodes can be reordered (meaning the temporal sequence is not important) without changing the network properties, while in recurrence plots and recurrence quantification analysis the temporal ordering of the states is fundamental.

Complex network measures can characterize the network nodes separately or the entire network as a whole, by local or global measures, e.g., for detecting different dynamical regimes or unstable periodic orbits (Marwan et al., 2009; Zou et al., 2010; Donner et al., 2011). An important measure is the *network transitivity*

$$\mathcal{T} = \frac{\sum_{i,j,k=1}^{N} A_{i,j} A_{j,k} A_{k,i}}{\sum_{i,j,k=1}^{N} A_{i,j} A_{k,i}}, \tag{12}$$

revealing the probability that two neighbours (i.e. recurrences) of any state are also neighbours (Barrat and Weigt, 2000). Intuitively, dynamics with fast diverging phase space trajectories will have a rather low probability that such triangle configurations of connected nodes retain for some time. In contrast, regular or periodic dynamics will exhibit a high probability of the occurrence of such triangles. Therefore, high values in $\mathcal{T}$ represent regular and low values an irregular dynamics (Zou et al., 2010), which is supported by the interpretation of this measure as being directly linked to a generalized notion of the effective spatial dimensionality of the network in phase space (Donner et al., 2011).

Another interesting network measure for recurrence analysis is the average length of shortest paths between all pairs of nodes, the *average path length*

Fig. 9. Recurrence network of the insolation time series as shown in Fig. 8A. The colour represents the time (the older the darker the colour).

$$\mathcal{L} = \frac{1}{N(N-1)} \sum_{i,j=1}^{N} \ell_{i,j}, \tag{13}$$

where the length of a shortest path $\ell_{i,j}$ is defined as the minimum number of links that have to be crossed to travel from node i to node j (Boccaletti et al., 2006). Disconnected pairs of nodes are not included in the average.

The confidence intervals for the network measures are estimated in a similar way as for the entropy measures. We create surrogate time series by bootstrapping values from the time series and calculate the network measures from the corresponding recurrence networks. By repeating this procedure many times, the empirical test distributions are created, which are then used to find the 5% and 95%-quantiles as the confidence interval.

The recurrence network approach was used to identify palaeoclimate regime transitions, such as the Plio-Pleistocene African climate variability and its relationship to human evolution (Donges et al., 2011b) or the Holocene variability of the Asian monsoon and its impact on ecosystems (Marwan and Kurths, 2015; Prasad et al., 2020) and ancient human societies (Donges et al., 2015a). Another application was investigating the link between the Indian and the East Asian monsoon (Feldhoff et al., 2012).

Further phase space based measures are available and can be useful. These include other RQA and recurrence network measures e.g., trapping time and mean average diagonal line length (Marwan et al., 2002), measures evaluating similarities in phase space such as FLUS (Malik et al., 2014), or entropy estimates, e.g., sample entropy (Richman and Moorman, 2000) or recurrence period density entropy (Little et al., 2007).

Software. The number of software packages for recurrence analyses is continuously increasing due to the increasing popularity of this method. Examples for Python are the *pyunicorn* package (Donges et al., 2015b) or the *PyRQA* package (Rawald et al., 2017), and for MATLAB the *CRP Toolbox* (Sect. 7, Table 4).

2.5. Visibility graphs

An alternative approach to transform time series to networks and to characterize them by their network properties is based on visibility graphs, originally introduced for the detection of obstacles by mutual visibility relationships between points in two-dimensional landscapes (e.g., for automatisation and architectural design) (Lacasa et al., 2008). Similar to recurrence networks, a network node represents a time point. A link $A_{ij} = 1$ is now defined by the rule

$$\frac{x_i - x_k}{t_k - t_i} > \frac{x_i - x_j}{t_j - t_i} \tag{14}$$

for all time points t_k with $t_i < t_k < t_j$, i.e., we can connect the values at t_i and t_j by a straight line without crossing another local peak in between them (Fig. 10). The topology of the visibility networks is related with fractal and multifractal properties of the underlying time series (Lacasa et al., 2009).

Another, even more interesting application of visibility networks is their ability to identify time irreversibility in time series. Time irreversibility is a typical indicator of nonlinear dynamics (Theiler et al., 1992). Visibility networks can be used to test for this specific type of dynamics, in particular to identify nonlinear regime shifts (Lacasa et al., 2012; Donges et al., 2013).

The basic idea is to compare the statistics of links coming from the past ($A_{j<i}$) or going into the future ($A_{j>i}$), referred to as retarded and advanced links (in the visibility network all links have a clear time direction). We can use the retarded and advanced degrees

$$k_i^r = \sum_{j<i} A_{ij}, \qquad k_i^a = \sum_{j>i} A_{ij}, \tag{15}$$

with $k_i = k_i^r + k_i^a$, or the clustering coefficient of the advanced and retarded links

$$C_i^r = \binom{k_i^r}{2}^{-1} \sum_{j<i,k<i} A_{ij}A_{jk}A_{ki}, \qquad C_i^a = \binom{k_i^a}{2}^{-1} \sum_{j>i,k>i} A_{ij}A_{jk}A_{ki}, \tag{16}$$

denoted as retarded and advanced cluster coefficients.

Given a stationary system, time reversibility means that the joint probability of a sequence of numbers is the same as the joint probability of the reversed version of this sequence (Lawrance, 1991). The probability distributions of the retarded and advanced degrees $\rho(k_i^r)$ and $\rho(k_i^a)$ would then not deviate much (same for C_i^r and C_i^a; Fig. 11). To test this, the distributions can be compared by a Kolmogorov-Smirnov (KS) test. This test statistic provides p-values $p(k)$ and $p(C)$ to assess whether the null-hypothesis of reversibility can be rejected (Donges et al., 2013).

This approach has been used to identify a nonlinear regime shift in the North Atlantic ocean circulation at the onset of the Little Ice Age (Schleussner et al., 2015), indicating a multi-stability in the Atlantic ocean circulation. Visibility graphs, in general, are useful tools for several classification and diagnostic purposes (Ahmadlou et al., 2010; Zou et al., 2014; Gao et al., 2016; Supriya et al., 2016).

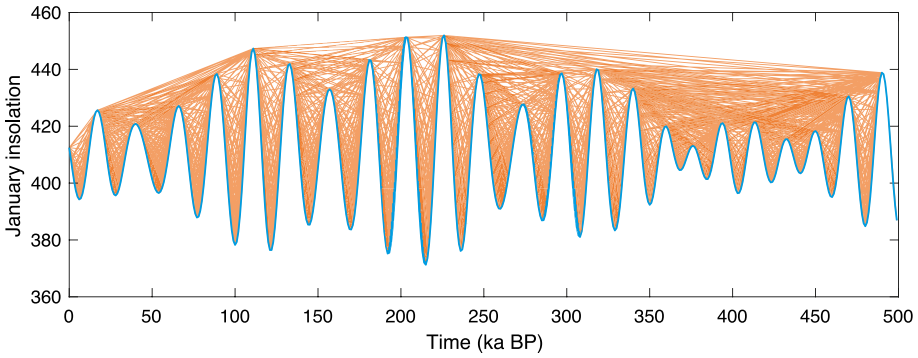

Fig. 10. Visibility graph of the insolation time series as shown in Fig. 8A.

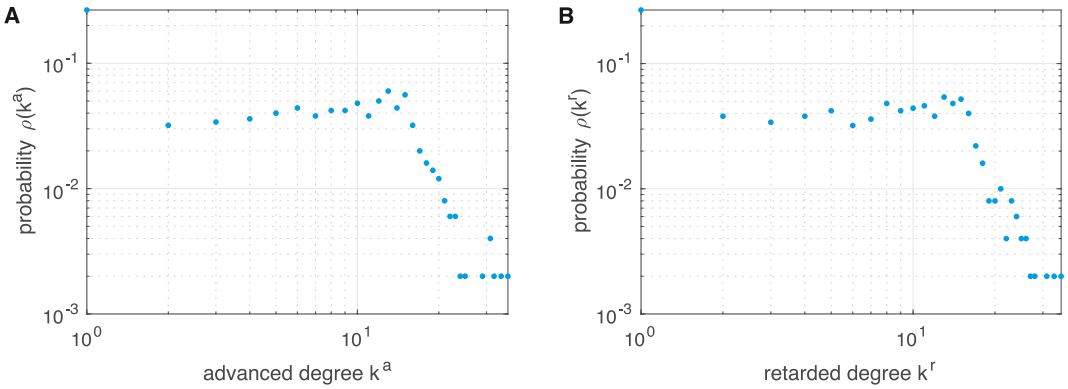

Fig. 11. Probability distributions of (A) advanced and (B) retarded degrees $\rho(k_i^a)$ and $\rho(k_i^r)$ of the visibility graph computed from the insolation time series as shown in Fig. 10. The KS-test reveals no significant difference between $\rho(k_i^a)$ and $\rho(k_i^r)$ by a p-value of 1.0, thus, the null hypothesis that the time series is reversible cannot be rejected.

Software. The *pyunicorn* package for Python provides tools for studying visibility graphs (and complex networks in general) (Donges et al., 2015b).

3. Data

Marine sediments provide insights into geological processes and are widely used to study the climatological and environmental conditions of the past (Westerhold et al., 2020). Here we consider marine records of different types of proxies for the long-term aridification (based on terrigenous dust flux) of the northern part of the African continent during the Plio-Pleistocene (Trauth et al., 2009; Donges et al., 2011a) and the variations in regional temperature and global ice volume (alkenone based SST and benthic δ^{18}O). Corresponding time series are derived from five sediment records (from West to East; Table 2, Figs. 12 and 13):

- ODP 662 (Atlantic Ocean west of equatorial Africa),
- ODP 659 (Atlantic Ocean offshore subtropical West Africa),

Table 2
Basic properties of the analysed palaeoclimate time series. N is the number of samples contained in the time series, $\langle \Delta T \rangle$ the mean sampling interval, and $\sigma(\Delta T)$ the standard deviation of sampling intervals (to illustrate the spread of the sampling intervals). The desired window size is $W^* = 410$ ka. W is the corresponding average number of sampling points covering this time span.

Record	N	Time span (Ma BP)	$\langle \Delta T \rangle$ (ka)	$\sigma(\Delta T)$ (ka)	W	Reference
ODP 662 SST	912	3.54–1.366	2.39	1.05	171	(Herbert et al., 2010)
ODP 659 dust flux	1221	5.0–0.002	4.10	2.69	100	(Tiedemann et al., 1994)
ODP 659 δ^{18}O	1170	5.0–0.002	4.28	2.88	95	(Tiedemann et al., 1994)
Medisect δ^{18}O	811	5.33–1.212	5.08	2.06	80	(Lourens et al., 1996)
ODP 967 dust flux	8417	3.028–0.0	0.36	0.31	1139	(Larrasoaña et al., 2003)
ODP 721 dust flux	2757	5.0–0.006	1.81	1.52	226	(deMenocal, 1995; DeMenocal, 2004)
ODP 722 SST	1680	3.33–0.007	1.98	0.89	207	(deMenocal, 1995; DeMenocal, 2004)

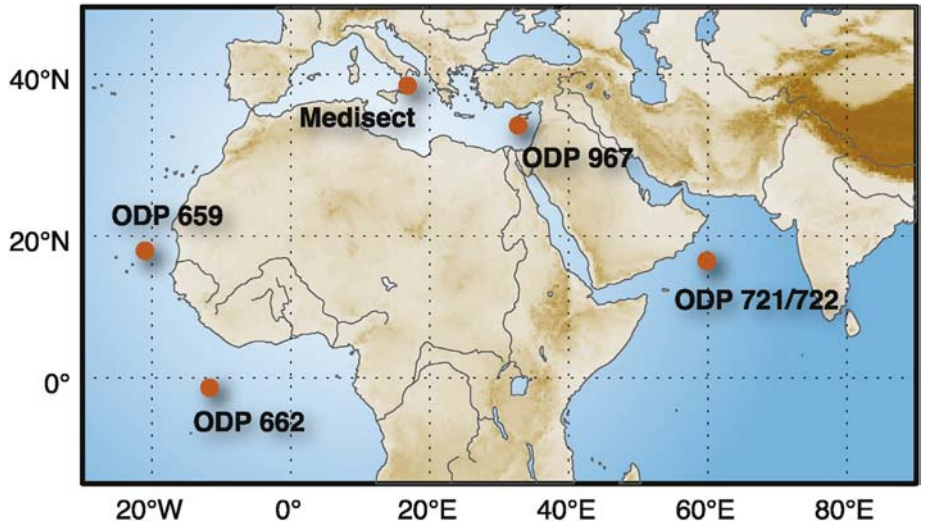

Fig. 12. Map of North Africa and surrounding ocean basins with indications of the archives used in this work.

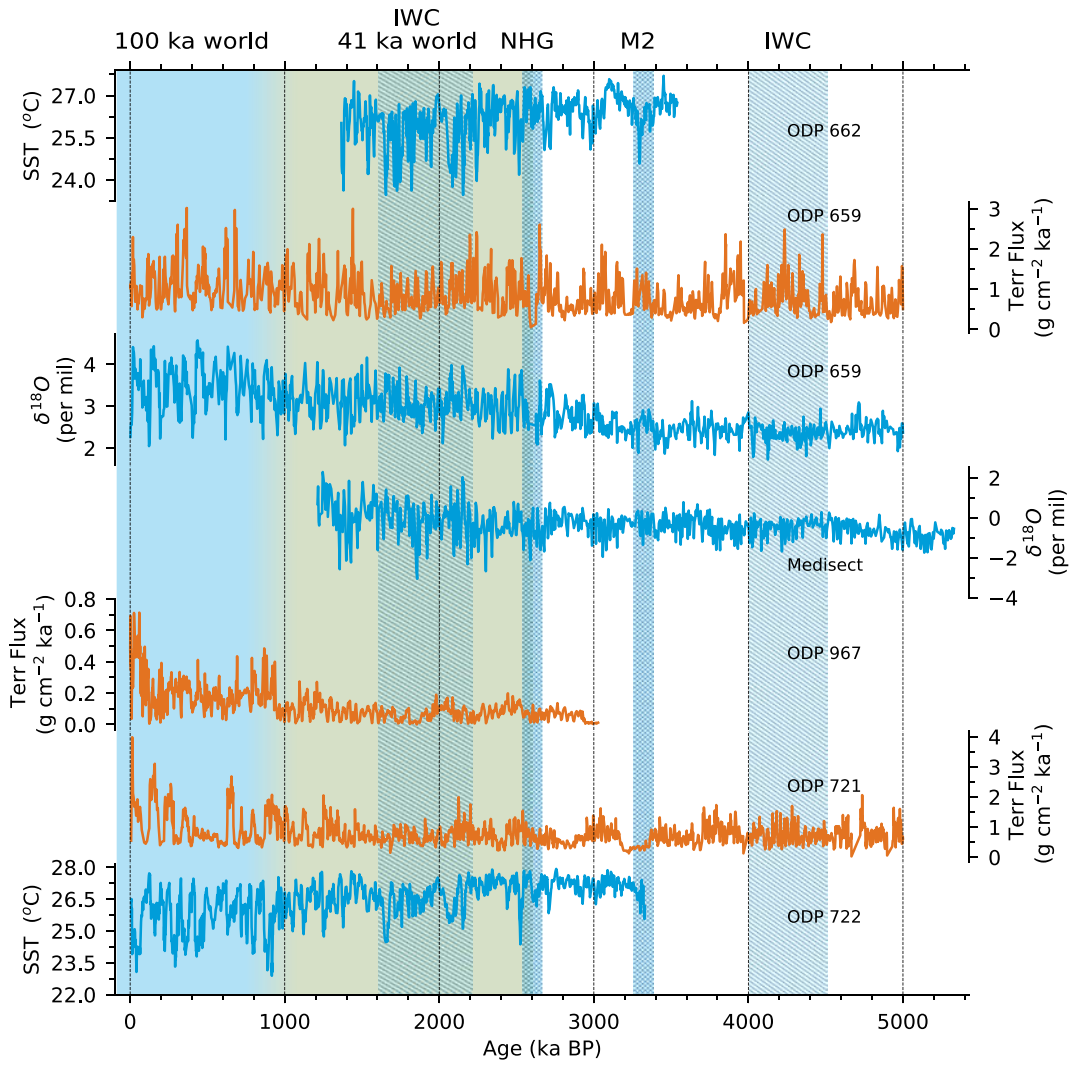

Fig. 13. Palaeoclimate time series used in this study (blue – temperature related proxies, orange – terrigenous dust flux proxies) and important climate regimes: IWC – intensified Walker circulation, marine isotope stage M2 with decreased global temperature, NHG – onset of northern hemisphere glaciation (transition from Pliocene to Pleistocene), 41 ka (green shaded) and 100 ka (blue shaded) dominated glacial cycles.

Table 3
Parameters used for the selected methods in this study (τ, $l_{\min}$, and $v_{\min}$ are in sampling time) .

Methods	Parameters
Shannon entropy	number of bins $N_{\text{bins}} = 20$
Order entropy	dimension $d = 3$, lag $\tau = 1$
Potential analysis	standard deviation stochastic process $\sigma = 1.5$
Recurrence analysis	fixed recurrence rate $RR = 0.05$, embedding dimension $m = 3$, embedding delay $\tau = 2$, $l_{\min} = 2$, $v_{\min} = 2$
Visibility graph	horizontal visibility
Windowing	window size $w = 410$ ka window step $ws = 41$ ka
Confidence interval	number of surrogates $N_{\text{surr}} = 5,000$ 5% and 95%-quantiles

- Medisect (Mediterranean on the south coast of Sicily and Calabria),
- ODP 967 (Eastern Mediterranean Sea),
- ODP 721/722 (Arabian Sea).

They have a sufficient temporal resolution of an average sampling time ranging from 0.4 ka up to 4.3 ka. A high temporal resolution is necessary for performing time series analysis (in particular for time-resolved/windowed analysis).

4. Results

We apply nonlinear time series analysis as described in Sect. 2 to the marine Plio-Pleistocene proxy records in order to investigate and characterize the dynamics of transitions between the wet and arid climate in the Northern part of Africa (considering the time scale given by the sampling, i.e., we discuss dynamical variations at time scales of $> 1,000$ years). Before we compare all proxy records, we will focus on one record (terrigenous dust flux proxy from ODP659) and explain our findings in more detail. The used parameters for the methods are provided in Table 3.

4.1. Results for dust flux proxy from ODP659

The studied measures of nonlinear time series analysis reveal different aspects regarding the dynamical properties. The measures are calculated within overlapping windows of length 410 ka (41 ka

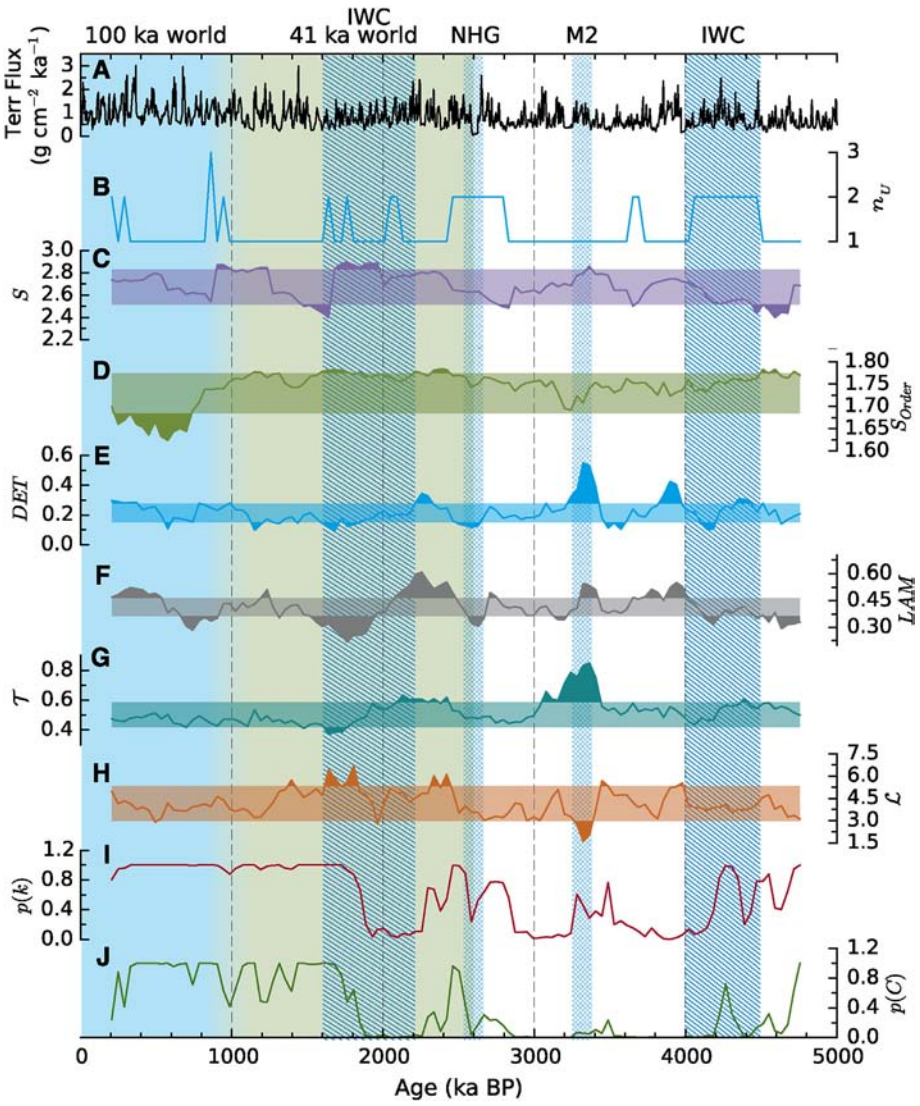

Fig. 14. Results for exemplary dust flux proxy record from ODP659 with the important climate regimes as in Fig. 13.

offset) to investigate changes in the dynamics (e.g., to identify regime transitions between more periods and more erratic climate variability). This implies that a single point in the resulting time series of measures corresponds to a period of 410 ka, two consecutive points correspond to 410 + 41 ka, and so on.

In the considered period, several known climate regime transitions occurred. The most prominent change is the transition from the Pliocene to the Pleistocene, around 2.6 Ma ago, with the onset of cyclical glaciations in the northern hemisphere (onset of northern hemisphere glaciation, NHG). During the Pliocene, a significant tropical climate reorganisation with the development of a strong Walker circulation (intensified Walker circulation, IWC) occurred between 4.5 and 4.0 Ma (Ravelo et al., 2004), and the marine isotope stage M2 with decreased global temperature occurred at 3.3 Ma (Lisiecki and Raymo, 2005). During the Pleistocene, the mid-Pleistocene transition (MPT) between 1.1 and 0.7 Ma is important, changing the glacial cycles from approximately 41 ka to a 100 ka dominant periodicity (Clark et al., 2006). In the course of the early Pleistocene between 2.2 and 1.5 Ma, another significant tropical climate reorganisation with intensification and spatial shift of the Walker circulation (IWC) occurred (Ravelo et al., 2004).

Potential analysis detects the number of potential wells from the time series, interpreted as the number of (stable) climate states. Singular excursions are neglected because the specific regimes should be identified over at least two consecutive windows to ensure the robustness of our results. The number of climate states n_U changes between one and two (Fig. 14B). For most of the time, there is only one stable climate state, according to potential analysis. Starting at 4.6 Ma, corresponding to the time of known large scale tropical atmospheric reorganisation, the African climate bifurcates to a two-state climate, lasting for approx. 800 ka (taking the window length into account), indicating that the climate system was alternating between two major climate states. A similar epoch can be found at the transition from the Pliocene to the Pleistocene between 2.8 Ma and 2.4 Ma and the MPT between 1.0 and 0.8 Ma. Further epochs with indicated double-well potential are too short-lived to be considered as reliable.

Next, the two entropy measures are calculated. The windowed Shannon entropy of the time series identifies changes in the amplitude distribution of the proxy values. In contrast, the order entropy considers the dynamics and, thus, identifies changes in the dynamics instead of the proxy's value distribution. The values of the Shannon entropy vary slightly between 2.4 and 2.9 (Fig. 14C). In order to interpret the variation as tending to larger or smaller

values, we apply a significance test based on a bootstrap-based confidence interval. Only entropy values outside the confidence interval will be interpreted as a significant increase or decrease. Significant smaller values indicating an unusually peaked amplitude distribution occur during the epoch between 4.8 and 4.5 Ma (before the tropical atmospheric reorganisation) and around 1.6 Ma (after the IWC); increased values, indicating a broader (less peaked) amplitude distribution, occur between 2.0 and 1.6 Ma and around 1.0 Ma, corresponding to IWC and the MPT, respectively. However, the values exceed the significance interval only slightly. The order entropy varies within the confidence interval up to the MPT at 0.8 Ma, after which it decreases significantly to lower values (Fig. 14D). Before this point of time, it only slightly increases indicating more complex dynamics during 4.8 and 4.6 Ma (before the tropical atmospheric reorganisation), around 2.4 Ma (at the onset of northern hemisphere glaciation), and during the tropical atmospheric reorganisation between 1.8 and 1.6 Ma. At the MPT 800 ka ago, the dynamics changed to significantly less complex dynamics.

In the following, we consider the measures related to recurrence analysis. The measure determinism (DET) significantly changes over time (Fig. 14E). A significant increase occurs between 4 and 3.8 Ma (after the period of stronger Walker circulation), between 3.4 and 3.2 Ma (during M2), and around 2.2 Ma (just after the onset of northern hemisphere glaciation). Less pronounced decreases occurred around 4.2 Ma (before the period of stronger Walker circulation), 3.5 Ma (before M2), 2.5 Ma (at the onset of glaciation), and between 1.8 and 1.6 Ma (during the IWC). The increased determinism values indicate intervals of more predictable (e.g., periodic) variability, whereas low values indicate a more random variation. Laminarity (LAM) shows significant increases similar as DET (Fig. 14F) after the period of stronger Walker circulation (between 4 and 3.8 Ma), during M2 (between 3.4 and 3.2 Ma), and during the onset of the glaciation (between 2.5 and 2 Ma). Additionally, after the MPT (after 500 ka), LAM again increases. Increased LAM can be an indication for more persistent dynamics. In contrast, significantly lower LAM values can be found before the period of stronger Walker circulation between 5 and 4.6 Ma, but also during the stronger Walker circulation between 2 and 1.6 Ma. At the MPT (between 1.0 and 0.6 Ma) the LAM is also lower than usual.

The (recurrence) network based measure transitivity $\mathcal{T}$ displays a similar behaviour as DET, with increased values during the M2 between 3.5 and 3.0 Ma and after the onset of the glaciation between 2.5 and 2.2 Ma; as well as a decrease during the period of IWC at around 1.8 Ma. Although this measure represents different nonlinear aspects of the dynamics, it can also be interpreted in the sense of more regular (larger values) or more random (low values) variability. The different regimes indicated by both measures during the same time intervals support the hypothesis of climatological changes between more variable and more regular climate variability. The average path length highlights the timing of the onsets of abrupt regime changes. This measure indicates abrupt changes at M2 (3.3 Ma), at the transition from the Pliocene to the Pleistocene (onset of NHG) and the Pleistocene IWC.

Finally, the temporally directed topological properties of the visibility graphs are used to test whether the considered periods behave like a nonlinear process (by testing for reversibility). This is performed by considering the p-values of the KS-test (Subsect. 2.5). Very small p-values indicate periods of time irreversibility or non-stationarity, suggesting nonlinear behaviour during these times. Both measures, based on degree and clustering coefficient, behave very similarly. Only during the time intervals after the IWC (after 4.0 Ma) and up to the M2 (3.3 Ma), between the M2 and the transition phase to the Pleistocene (3.2–2.8 Ma), as well as during the time after the IWC (between 2.2 and 1.8 Ma), the time reversibility had to be rejected, suggesting more nonlinear behaviour. Overall, a pattern emerges indicating more nonlinear climate dynamics (more complex) before approx. 2.0 Ma during the Pliocene and early Pleistocene, and more linear variability (less complex) during the Mid- and late Pleistocene.

4.2. Unified view on North African Plio-Pleistocene climate

In the following, we will investigate and discuss the dynamics of the dust flux and SST proxy records using the selected measures order entropy (S_{order}), number of states (n_U), determinism (DET), and time reversibility ($p(\mathcal{C})$). The proxy time series reflect conditions of regional temperature (provided by Alkenone based SST estimations and δ^{18}O) and African aridity (terrigenous dust flux) at different locations.

Order entropy. The order entropy of the tropical SST records reveals an increase in the complexity of the temperature dynamics in the subtropics during the IWC (Fig. 15A, G). The δ^{18}O temperature proxy from the ODP659 site presents a similar increase in complexity during the Pliocene IWC, but not during the Pleistocene IWC (Fig. 15C). At the Medisect region, S_{order} does not show any (significant) influence of the IWC on the climate dynamics (Fig. 15D).

The dynamical complexity of the dust flux records shows regional differences. During the Pliocene IWC, the complexity is slightly increased in the Arabian sea (Fig. 15F), while it is less affected in the subtropical Atlantic (Fig. 15B). During the Pleistocene IWC, the dynamical complexity is only slightly increased at the end of the corresponding time interval, when the large-scale atmospheric circulation pattern is changing to less intensive Walker circulation. In contrast, in the eastern Mediterranean, the complexity is even significantly reduced (Fig. 15E).

During the M2 cooling event, the complexity in the dynamics in all proxies and sites covering this event is reduced (Fig. 15B, C, D, F).

The onset of northern hemisphere glaciation is related to a short and slight increase in the dynamical complexity of the dust flux in the tropical Atlantic and in the eastern Mediterranean (Fig. 15B, E), but a decrease of complexity in the Arabian sea (Fig. 15F). This reduced complexity due to the glacial cycles is also visible in the SST proxy of the tropical Atlantic (Fig. 15A), but not in the northern subtropical Atlantic or the Arabian sea (Fig. 15C, G). This is a sign for a reorganisation of the atmospheric circulation pattern due to the beginning of the glaciation, a pattern that is later changed again during the Pleistocene IWC.

The transition from the 41 ka to the 100 ka dominated glaciation cycles after the MPT is related to a reduction of the dynamical complexity in the dust flux records (Fig. 15B, E, F). In the eastern Mediterranean, this happens later than in the Arabian sea.

Potential analysis. The potential analysis reveals an increase in the number of states during the IWC (Fig. 16). Here we can find slight differences between the regions and proxies. During the Pliocene, this increase is most clearly visible in the west, in the dust flux record, and less clear in the east, but opposite during the Pleistocene (Fig. 16B, E, F).

The potential analysis of the SST proxy in the Arabian sea shows different results than for the other SST proxies. It suggests more states after the onset of glaciation, but a reduced number of states during the IWC (Fig. 16A, D, G), which can be a sign of a different ocean circulation regime in the Indian Ocean during this time.

Recurrence analysis. The recurrence plot based determinism measure shows clear differences in the absolute values of the SST proxies (<0.5) and the terrigenous dust flux records in the Arabian sea and the eastern Mediterranean, with values up to 0.98 in the ODP967 record. The ODP967 record should be considered a bit different here, because larger temporal resolution (as it is the case

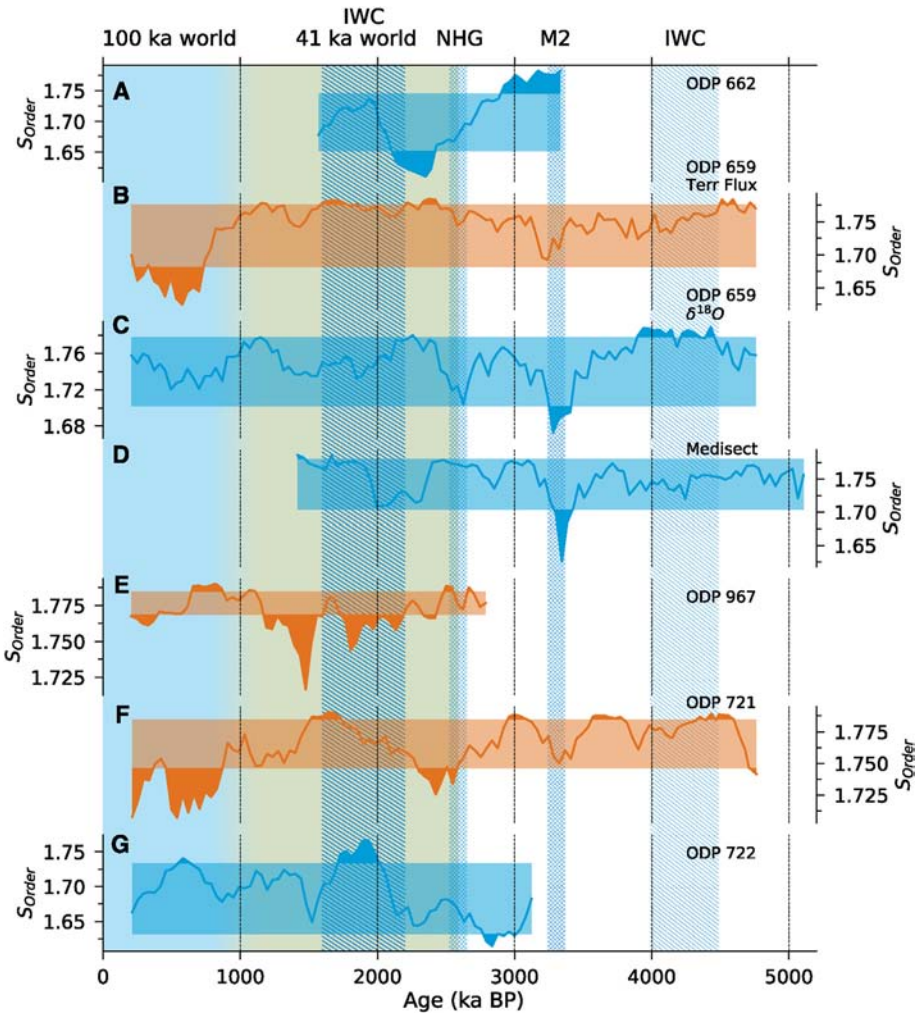

Fig. 15. Order entropy (or permutation entropy) of the analysed palaeoclimate proxy series.

in ODP967) is causing more longer lines in recurrence plots and shifts DET towards larger values. Therefore, by using the significance test we discuss the variation in DET in a relative way.

We find an increase to more predictable dynamics (as typical for periodic or cyclic dynamics) after the onset of the cyclical NHG in the terrigenous dust flux records in the eastern Mediterranean and the subtropical Atlantic (Fig. 17B, E), but also in the SST dynamics of the Medisect site, and slight or tending increase (although partly not significant) in the tropical Atlantic and the Arabian sea (Fig. 17A, D, G).

The M2 event is also characterised by more predictable variability of the dust flux records (Fig. 17B, F), but does not affect the dynamics of the temperature dynamics in general (Fig. 17A, D), except for the subtropical Atlantic (those DET values are in general quite low, Fig. 17C).

During the Pleistocene IWC, the dust flux in the eastern Mediterranean shows a remarkable increase in the DET values (Fig. 17E), confirming the finding based on order entropy that the dynamics becomes more regular and predictable.

After the MPT, the dynamics becomes remarkably more predictable in the Arabian sea, but less predicable in the eastern Mediterranean (Fig. 17E and F). Interestingly, the site ODP659 does not show significant change in this respect, although the order entropy has shown a decrease of dynamical complexity in this region, too (Figs. 17B and 15B).

Time reversibility (nonlinearity) test. The test for time reversibility as an indicator of nonlinearity (based on $p(\mathcal{C})$) of the proxy records shows regional differences. In the tropical west, a nonlinear behaviour in the temperature (SST) dynamics is only indicated after NHG onset and lasting until the Pleistocene IWC (Fig. 18A). In the subtropical west, there is almost no significant p-value for the SST nonlinearity, except for very short times at the M2 event and in the second half of the Pleistocene IWC (Fig. 18C). In the Mediterranean region, nonlinear dynamics is indicated before and during the M2 event, as well as before the onset of the NHG (Fig. 18D). In the Arabian sea, we only find nonlinear behaviour for the SST dynamics just before and after the MPT (Fig. 18G).

The analysis of the terrigenous dust flux records indicates short periods of nonlinear behaviour before and during the Pliocene IWC and during the Pleistocene IWC (Fig. 18B, F), whereas the East Arabian site responds later than the western site. In contrast, we do not find such a nonlinear dynamics in the eastern Mediterranean during the Pleistocene IWC (Fig. 18E), but before and after this IWC. After the M2 cooling event, nonlinear behaviour in the dust flux records is found in the East Arabian sea and the subtropical Atlantic.

5. Discussion

The considered methods of nonlinear time series analysis reveal different aspects of Africa's aridification and regional temperature

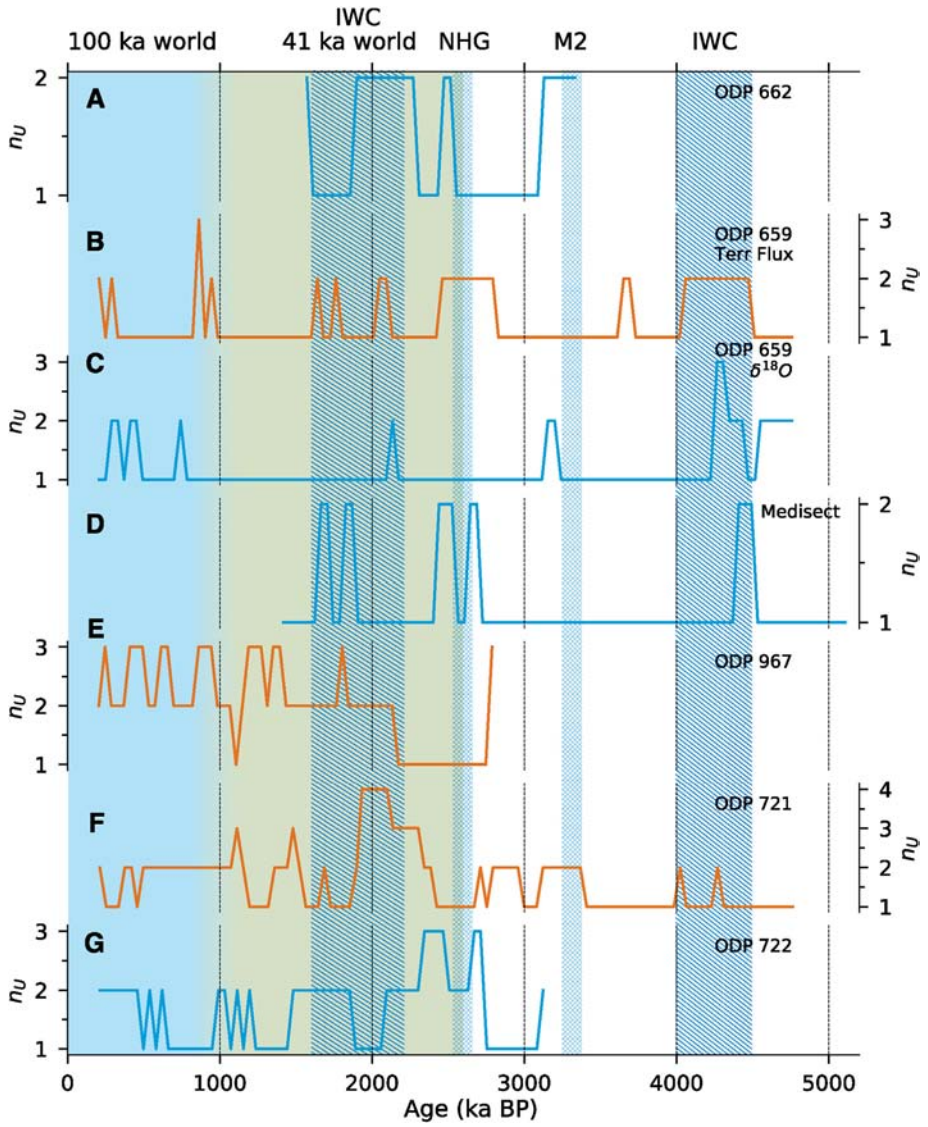

Fig. 16. Potential analysis of the analysed palaeoclimate proxy series.

variations during the Plio-Pleistocene. When directly comparing the corresponding measures, we find that they are not or only slightly correlated to each other (Fig. 19), but allow us to interpret them from a dynamical point of view by providing complementary information, as we discuss in more detail below for several key climate events in this epoch (as mentioned above, the dynamical variation discussed here occurs at time scales $> 1,000$ years).

Intensified Walker circulation (IWC). The IWC appears to be generally related to a dynamics with a larger number of possible quasi-stable states, in Africa's aridity (represented by the proxy records at ODP659 and ODP721) as well as in the regional temperature (indicated by n_U). The transition to this regime during the Pliocene is characterised by a significant change in the amplitude distributions of the dust flux data from less to more complex amplitude distributions (indicated by elevated S for ODP659), corresponding to the increased number of states. Similarly, during the Pleistocene, we find a transition from high to low complexity amplitude distribution when this specific regime terminated. During the onset of the Pliocene IWC period, we find slight but significant increases of the complexity in the dynamics during the transition phase in African hydro-climate as represented by ODP659 and ODP721 (indicated by increased S_{order}). Similar to the change in the amplitude distributions at the termination of the Pleistocene IWC, we find a drop in the complexity of the dynamics at this transition. The IWC also comes along with a shift from more regular, predictable, and persistent dynamics to less regular, less predictable, and less persistent dynamics ($\mathcal{T}$, DET, LAM). Moreover, the Pleistocene IWC seems to behave rather nonlinear, whereas during the Pliocene IWC this cannot be clearly identified, although a tendency is visible (indicated by low $p(k)$ and $p(C)$ values). Overall,

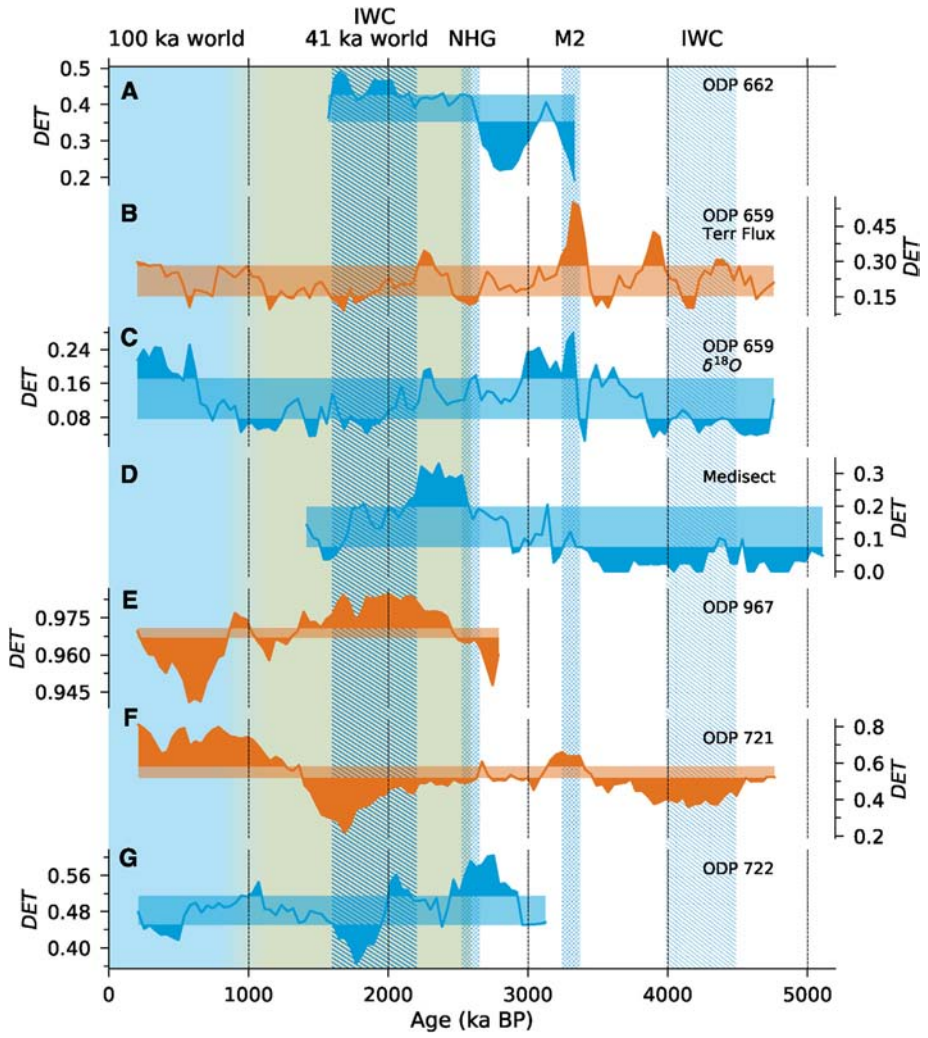

Fig. 17. Determinism measure of the analysed palaeoclimate proxy series.

these results suggest that the IWC is related to a 2-state regime in African climate (e.g., alternating between wetter and drier conditions), confirmed by the more complex amplitude distribution and the nonlinear behaviour, as well as with a less predictable and less persistent dynamics.

The terrigenous dust flux record at ODP site 967 (eastern Mediterranean) covers only the Pleistocene IWC and differs from the above observations. In contrast to the subtropical Atlantic and Arabian sea site, the eastern Mediterranean shows a remarkable increase in regularity and predictability during the IWC (low S_{order} and large DET), suggesting a change in the tropical rainbelt.

Based on the δ^{18}O and SST proxies, we also find clear spatial differences in the temperature dynamics in the Atlantic, Mediterranean, and Arabian sea regions. With beginning IWC, in the (sub-) tropical Atlantic the number of states is increasing whereas it is decreasing in the Arabian sea. At the same time, temperature dynamics becomes less predictable and less regular during the Pleistocene IWC in all regions.

Marine isotope stage M2. The marine isotope stage M2 is a relatively short period of colder global climate. It is related to more predictable and persistent dynamics in Africa's hydro-climate (low S_{order} and large DET, LAM, and $\mathcal{T}$). The subtropical Atlantic and Mediterranean temperature variability is also becoming less complex and more predictable (low S_{order}, increase in DET to intermediate and larger values).

In contrast, the tropical Atlantic shows a more complex and much less predictable dynamics during the M2 event (high S_{order} and low DET).

Following M2, the dynamics of African hydro-climate becomes again less predictable (average values of DET, LAM, and $\mathcal{T}$) and more nonlinear (indicated by $p(k)$ and $p(\mathcal{C})$).

These results could be interpreted in the sense that the cooling event has caused some cyclical variation between cold and warm temperatures in the northern hemisphere (anticipating the glacial

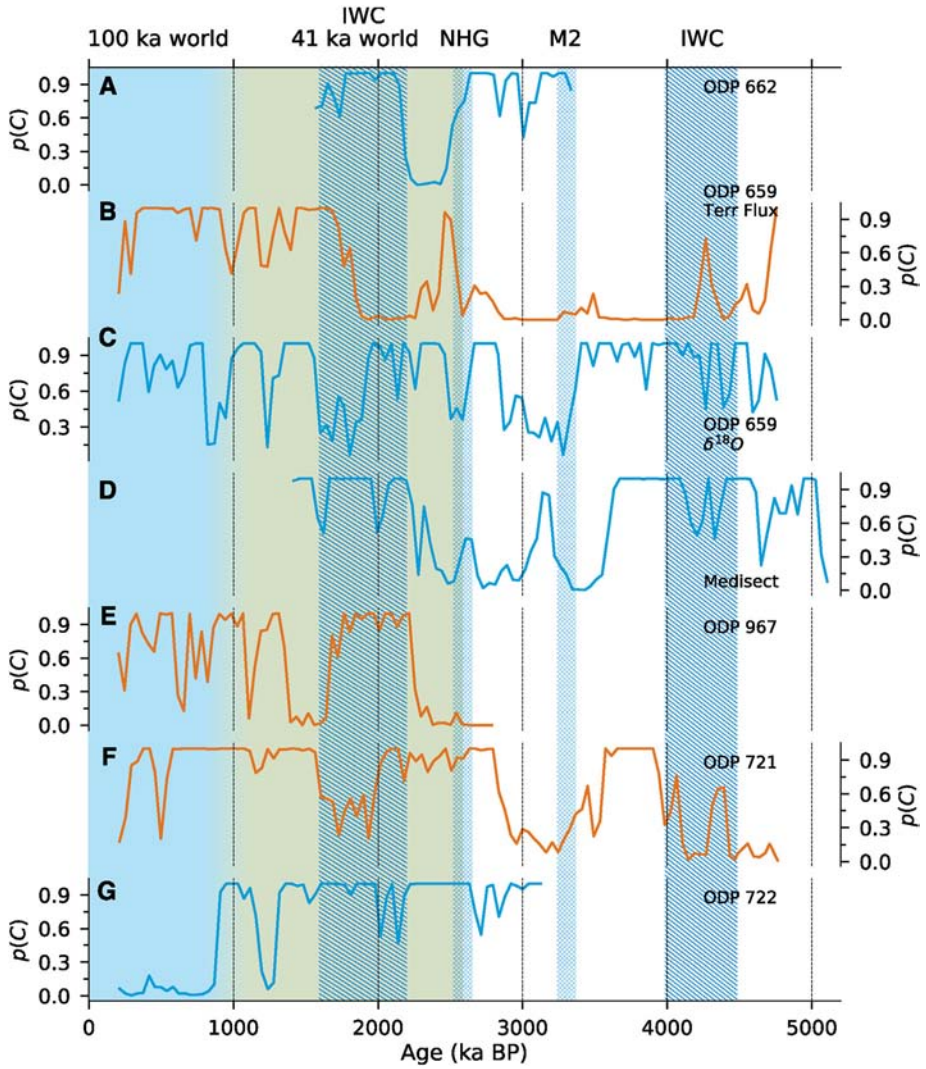

Fig. 18. Time series irreversibility indicator based on *p*-values of the visibility graph clustering coefficients for the analysed palaeoclimate proxy series (only very small *p*-values indicate significance).

oscillations at high latitudes during the late Pleistocene) and wet and dry climate in Africa, whereas in the tropics, no such cyclical changes occurred. However, the differences between these were not strong enough to cause a bifurcation of the system with two clearly different emerging states.

Onset of northern hemisphere glaciation. During the transition from Pliocene to Pleistocene, African hydro-climate dynamics clearly shifts to a less predictable and less persistent regime (low DET values). This appears to be related to a short-lived shift to more regular and less complex dynamics in the Arabian sea. After this transition phase, the dynamics becomes clearly more predictable and persistent in African hydro-climate, the tropical Atlantic, the Mediterranean region, and the Arabian sea, mainly as a result of the onset of cyclical glaciations.

Mid-Pleistocene transition (MPT). The MPT is characterised by a change from more to less complex amplitude distributions (indicated by S in the ODP659 dust record), and by a decrease in dynamical complexity (indicated by significant drop in S_{order}). Around the time of the transition, the co-occurrence of 41 ka and 100 ka cycles (Trauth et al., 2009) causes an increase in the number of possible system states (increase in n_U to 2 and even 3 in the dust flux proxies) and a less persistent dynamics (decreased LAM). After 500 ka, the dynamics becomes more and more predictable and persistent as the 100 ka cycles become more and more dominant (increasing DET values, decreasing S_{order}, except for the eastern Mediterranean). Consistently, climate variability is largely time reversible, indicating dominance of rather linear dynamics (large values of $p(k)$ and $p(\mathcal{C})$), with the remarkable exception of the Arabian sea, which shows a more nonlinear behaviour during the 100 ka world.

The MPT has not only changed the dynamics from a dominance of 41 ka to 100 ka cyclicity, but also caused a regime change in the

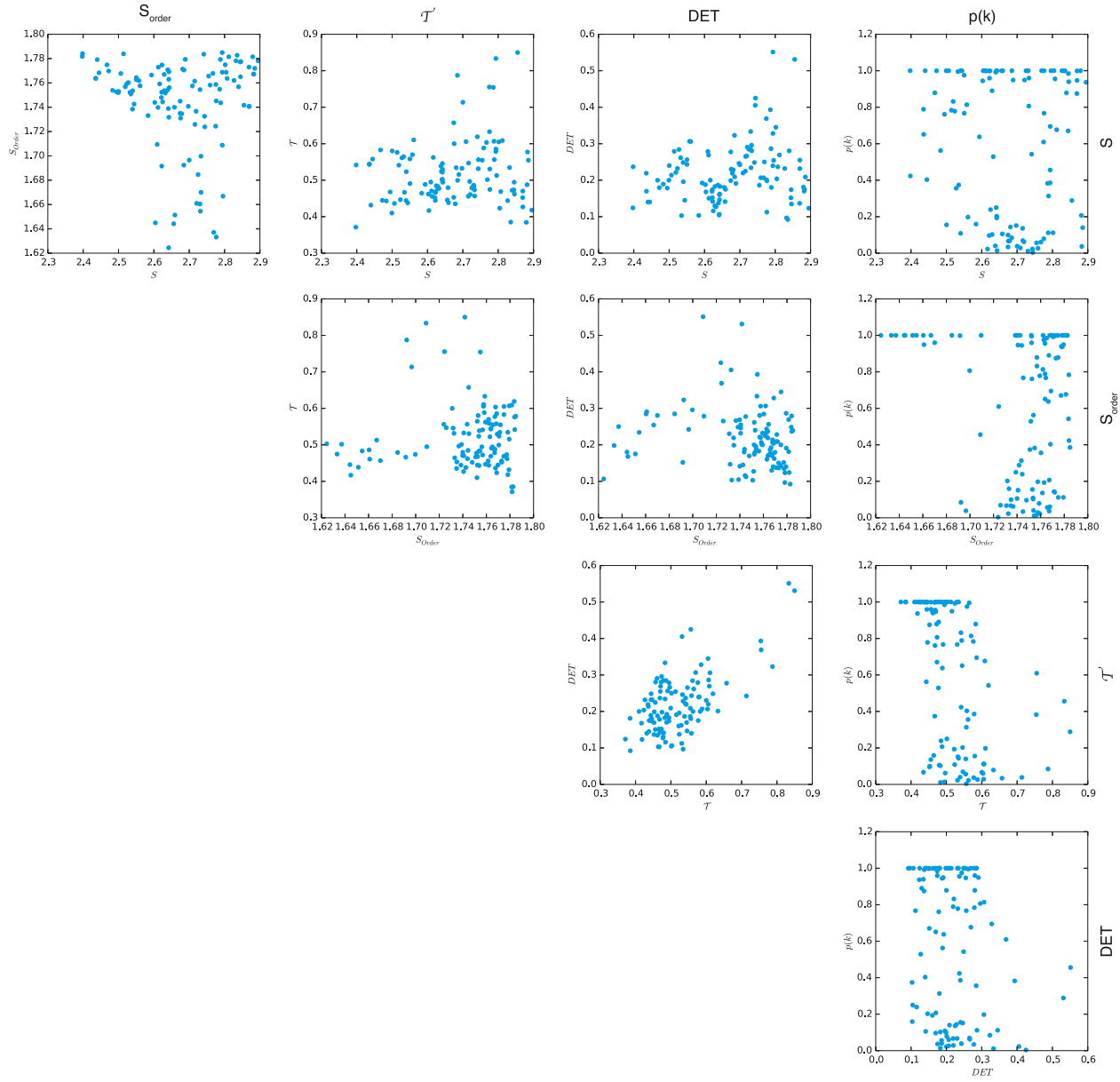

Fig. 19. Comparison of selected measures of nonlinear time series analysis for the terrigeneous dust flux record ODP659 (scatter plots).

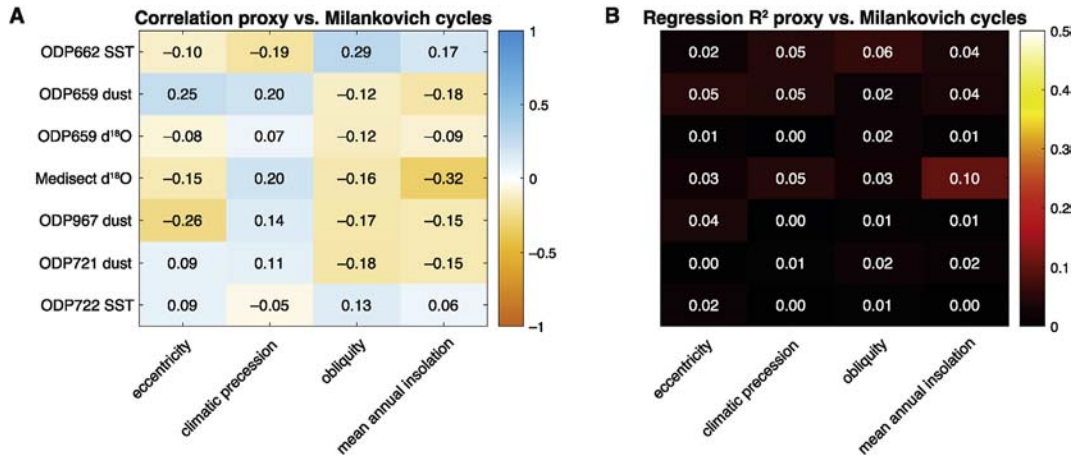

Fig. 20. (A) Pearson correlation and (B) coefficient of determination (R^2) between the original proxy data and the Milankovich cycles (interpolated to the time axis of the corresponding proxy), indicating no pronounced linear relationship between proxies and Milankovich cycles.

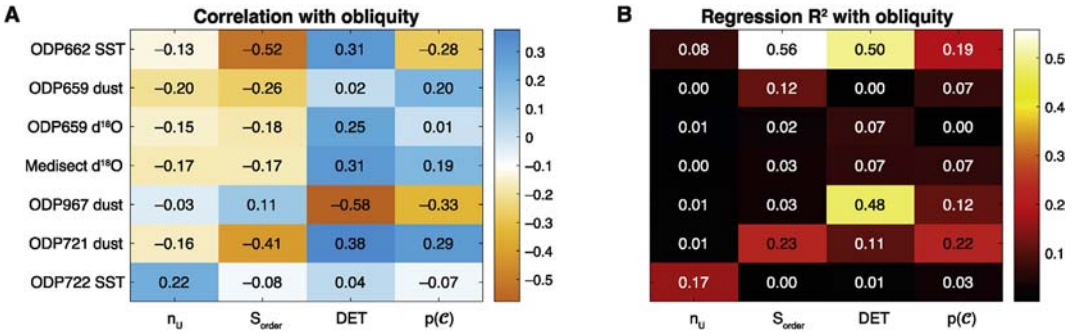

Fig. 21. (A) Pearson correlation and (B) coefficient of determination (R^2) between selected quantifiers of nonlinear time series analysis and the obliquity cycles (interpolated to the time axis of the corresponding proxy), indicating significant relationships between some of the dynamical regime changes in temperature and African hydro-climate and the seasonality inducing obliquity variation.

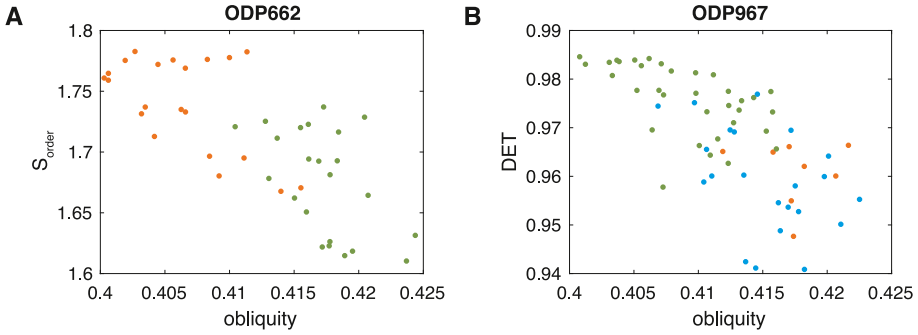

Fig. 22. (A) Pearson correlation and (B) coefficient of determination (R^2) between selected quantifiers of nonlinear time series analysis and and the obliquity cycles (interpolated to the time axis of the corresponding proxy), indicating a significant relationship between some of the dynamical regime changes in the temperature and African's hydroclimate and the seasonality inducing obliquity variation. The colour represents the Pliocene (orange), early Pleistocene before the MPT (green) and the late Pleistocene after the MPT (blue).

Arabian sea towards more nonlinear dynamics by additional influences, e.g., by cooling-warming cycles and changes in the meridional overturning circulation in the Indian ocean, or increased Indonesian throughflow after the MPT (Petrick et al., 2019).

The nonlinear analysis applied here covers different aspects, such as properties of the proxies' windowed amplitude distributions, complexity and predictability of the dynamics, nonlinear vs. linear dynamics, or multi-stability. As described above, such properties can change on longer time scales. One of the most important drivers of those climate regime changes are orbital variations in insolation in the form of Milankovich cycles, as is already obvious from the indicated dynamical changes when northern hemisphere glaciation sets in or when glacial cycles change from 41 to 100 ka dominant periodicity. This relationship is not directly visible in the proxy data, e.g., when applying linear methods, such as correlation and regression analysis (Fig. 20).

In contrast, several measures of nonlinear time series analysis are more clearly related to the Milankovich cycles (Figs. 14–18). Comparing the individual components of the Milankovich cycles, we find that the variation of obliquity is significantly correlated to several regime shift indicators, in particular for the proxies from ODP662 and ODP967 (Fig. 21). A larger obliquity causes more pronounced seasonality and its change triggers the onset of interstadials and stadials. A closer look at the relationship with obliquity reveals differences in the dynamical properties between the Pliocene, the early Pleistocene before the MPT, and the later Pleistocene after the MPT (Fig. 22). During the Pleistocene, the dynamics is more regular and predictable (increasing DET), due to the more cyclical variations (glacial cycles).

Moreover, we find spatial differences in the dynamics represented by the terrigenous dust flux proxies (e.g., Fig. 21A). The site in the eastern Mediterranean behaves mainly opposite to the site in the Atlantic and the Arabian sea. This result suggests a specific pattern in atmospheric circulation or the tropical rainbelt the change of which is affecting the subtropical regions east and west of Africa differently than in the north.

While these measures of nonlinear time series analysis reveal interesting insights in the changing climate dynamics, there are some important methodological aspects to be considered (Marwan,

2011). Entropy measures and potential estimation rely on good estimates of probability density functions and, thus, require long time series. Recurrence and network based methods can be applied on shorter time series, but may be biased by missing data or irregular sampling as it is common in palaeoclimate data. As we have seen, higher temporal resolution can shift values in certain measures (e.g., in DET). This is not a problem as long as we compare the variations only within a single record in a relative manner (as performed in this study). If direct comparison of absolute values is required, the data needs to be resampled to a common time axis. New approaches to reduce the biases induced by irregular sampling and simple interpolation approaches have been suggested, using time slotting, Gaussian kernel based interpolation, or transformation cost approaches (Babu and Stoica, 2010; Rehfeld et al., 2011; Ozken et al., 2015; Eroglu et al., 2016). The phase space reconstruction by time delay embedding as employed in this study can also cause spurious correlations, leading to an overestimation of deterministic dynamics. Therefore, alternative embedding concepts could play an increasing role in the future (Lekscha and Donner, 2018; Kraemer et al., 2021). Further bias can be caused by dating uncertainties and tuning to a target signal, e.g., astronomical tuning to the Milankovich cycles. The latter, in particular, is a serious problem when performing spectral or wavelet analysis (Blaauw, 2012). Although this tuning can also change the spatial distribution of line structures in recurrence plots, it is not a problem for recurrence quantification analysis, because it is based on the distribution of the line lengths, which is not strongly affected by the tuning. Nevertheless, novel definitions of recurrences, which even incorporate uncertainties (such as those coming from dating), might receive interest in the future also for palaeoclimate studies (Goswami et al., 2018). The synthesis of a large number of palaeoclimate records is not a simple task and can lead to confusing results. Complex networks can provide the necessary abstraction level that helps to declutter and highlight relevant spatial and process relationships (Rehfeld et al., 2013; Boers et al., 2021). For such purposes, we might also be interested in the interrelationships or directed couplings between those records. Usually, different sampling resolutions and dating uncertainties are a major problem which impedes the application of methods such as Pearson correlation, information transfer, synchronization analysis, or Granger causality. Although new approaches have been suggested in the last years which try to overcome these challenges, the results should be considered with care (Hannisdal, 2011; Rehfeld et al., 2011; Smirnov et al., 2017). Finally, the interpretability of the obtained results may depend crucially on the palaeoclimate archive or proxy under study, related to the observability of the proxy variable presenting a nonlinear transformation of the (usually unknown) climatic driver (Lekscha and Donner, 2020). But this is a general problem and applies to any statistical analysis of palaeoclimate proxy records.

6. Conclusions

In this review we have considered selected approaches from nonlinear time series analysis and applied them to marine palaeoclimate proxy records of African climate variations during the Plio-Pleistocene. We have shown that these methods reveal different aspects in the dynamics of the palaeoclimate and complement each other. In general, this approach can be used to study palaeoclimate regime changes. We have illustrated this approach by identifying and characterising changes in palaeoclimate during the Plio-Pleistocene, associated to significant events and transitions such as the marine isotope stage M2, the onset of the northern hemisphere glaciation, and the mid-Pleistocene transition. Compared to linear analysis or simple interpretations in terms of cooling and stadial-interstadial cycles, nonlinear time series analysis provides deeper insights into the dynamics, such as increasing or decreasing number of climate states (multi-stability), nonlinear vs. linear behaviour, or increasing predictability of the variation due to more cyclical dynamics. The synthesis of the nonlinear time series analysis of different proxy records can be used to make inferences on spatial differences in the impact of global climate drivers such as orbital variations and in changes in large-scale atmospheric patterns.

7. Data and software availability

The data and analysis script used here are available at Zenodo: https://doi.org/10.5281/zenodo.5578298.

Table 4
Web addresses of selected software packages providing the methods of nonlinear time series analysis similar to this study.

Method	Software	Language	URL
Entropy	CRP Toolbox	MATLAB	https://tocsy.pik-potsdam.de/CRPtoolbox/
Order entropy	ordpy	Python	https://github.com/arthurpessa/ordpy
	Permutation entropy	MATLAB	https://mathworks.com/matlabcentral/fileexchange/44161-permutation-entropy-fast-algorithm
Stochastic modelling	scipy	Python	(standard package)
	kramersmoyal	Python	https://github.com/LRydin/KramersMoyal
	Statistics and Machine Learning Toolbox	MATLAB	(standard package)
	FilterPy	Python	https://github.com/rlabbe/filterpy
Recurrence plots, recurrence networks	pyunicorn	Python	https://github.com/pik-copan/pyunicorn
	PyRQA	Python	https://pypi.org/project/PyRQA/
	CRP Toolbox	MATLAB	https://tocsy.pik-potsdam.de/CRPtoolbox/
Visibility graphs	pyunicorn	Python	https://github.com/pik-copan/pyunicorn

Declaration of competing interest

The authors declare that they have no known competing financial interests or personal relationships that could have appeared to influence the work reported in this paper.

Acknowledgement

This study was supported by the DFG projects MA4759/8–1 "Impacts of uncertainties in climate data analyses (IUCliD)", MA4759/9–1 "Recurrence plot analysis of regime changes in dynamical systems", MA4759/11–1 "Nonlinear empirical mode analysis of complex systems: Development of general approach and application in climate", by TÜBİTAK (Grant No. 118C236), by the BAGEP Award of the Science Academy, by the Leibniz Association (project DominoES), and the European Research Council (project ERA, ERC-2016-ADG-743080).

References

Afsar, O., Tirnakli, U., Kurths, J., 2016. Entropy-based complexity measures for gait data of patients with Parkinson's disease. Chaos: Interdisciplin. J. Nonlinear Sci. 26, 023115. https://doi.org/10.1063/1.4942352.

Ahmadlou, M., Adeli, H., Adeli, A., 2010. New diagnostic EEG markers of the Alzheimer's disease using visibility graph. J. Neural. Transm. 117, 1099–1109. https://doi.org/10.1007/s00702-010-0450-3.

Albeverio, S., Jentsch, V., Kantz, H. (Eds.), 2006. Extreme Events in Nature and Society. The Frontiers Collection. Springer Berlin Heidelberg, Berlin, Heidelberg. https://doi.org/10.1007/3-540-28611-X.

Babu, P., Stoica, P., 2010. Spectral analysis of nonuniformly sampled data – a review. Digit. Signal Process. 20, 359–378. https://doi.org/10.1016/j.dsp.2009.06.019.

Balasis, G., Daglis, I.a., Papadimitriou, C., Kalimeri, M., Anastasiadis, A., Eftaxias, K., 2008. Dynamical complexity in D_{st} time series using non-extensive Tsallis entropy. Geophys. Res. Lett. 35, L14102. https://doi.org/10.1029/2008GL034743.

Balasis, G., Donner, R.V., Potirakis, S.M., Runge, J., Papadimitriou, C., Daglis, I.A., Eftaxias, K., Kurths, J., 2013. Statistical mechanics and information-theoretic perspectives on complexity in the earth system. Entropy 15, 4844–4888. https://doi.org/10.3390/e15114844.

Bandt, C., Pompe, B., 2002. Permutation entropy - a complexity measure for time series. Phys. Rev. Lett. 88, 174102. https://doi.org/10.1103/PhysRevLett.88.174102.

Bandt, C., Shiha, F., 2007. Order patterns in time series. J. Time Anal. 28, 646–665. https://doi.org/10.1111/j.1467-9892.2007.00528.x.

Barrat, A., Weigt, M., 2000. On the properties of small-world network models. Eur. Phys. J. B 13, 547–560. https://doi.org/10.1007/s100510050067.

Blaauw, M., 2012. Out of tune: the dangers of aligning proxy archives. Quat. Sci. Rev. 36, 38–49. https://doi.org/10.1016/j.quascirev.2010.11.012.

Boaretto, B.R.R., Budzinski, R.C., Rossi, K.L., Prado, T.L., Lopes, S.R., Masoller, C., 2021. Evaluating temporal correlations in time series using permutation entropy, ordinal probabilities and machine learning. Entropy 23, 1025. https://doi.org/10.3390/e23081025.

Boccaletti, S., Latora, V., Moreno, Y., Chavez, M., Hwang, D.U., 2006. Complex networks: structure and dynamics. Phys. Rep. 424, 175–308. https://doi.org/10.1016/j.physrep.2005.10.009.

Boers, N., Kurths, J., Marwan, N., 2021. Complex systems approaches for Earth system data analysis. J. Phys.: Complexity 2, 011001. https://doi.org/10.1088/2632-072X/abd8db.

Boers, N., Rypdal, M., 2021. Critical slowing down suggests that the western Greenland Ice Sheet is close to a tipping point. Proc. Natl. Acad. Sci. Unit. States Am. 118, e2024192118. https://doi.org/10.1073/pnas.2024192118.

Boettner, C., Klinghammer, G., Boers, N., Westerhold, T., Marwan, N., 2021. Early-warning signals for cenozoic climate transitions. Quat. Sci. Rev. https://doi.org/10.1016/j.quascirev.2021.107177.

Brugger, J., Feulner, G., Petri, S., 2017. Baby, it's cold outside: climate model simulations of the effects of the asteroid impact at the end of the Cretaceous. Geophys. Res. Lett. 44, 419–427. https://doi.org/10.1002/2016GL072241.

Burke, K.D., Williams, J.W., Chandler, M.A., Haywood, A.M., Lunt, D.J., Otto-Bliesner, B.L., 2018. Pliocene and Eocene provide best analogs for near-future climates. Proc. Natl. Acad. Sci. Unit. States Am. 115, 13288–13293. https://doi.org/10.1073/pnas.1809600115.

Cao, L., 1997. Practical method for determining the minimum embedding dimension of a scalar time series. Physica D 110, 43–50. https://doi.org/10.1016/S0167-2789(97)00118-8.

Clark, P.U., Archer, D., Pollard, D., Blum, J.D., Rial, J.A., Brovkin, V., Mix, A.C., Pisias, N.G., Roy, M., 2006. The middle Pleistocene transition: characteristics, mechanisms, and implications for long-term changes in atmospheric pCO2. Quat. Sci. Rev. 25, 3150–3184. https://doi.org/10.1016/j.quascirev.2006.07.008.

Dakos, V., Scheffer, M., van Nes, E.H., Brovkin, V., Petoukhov, V., Held, H., 2008. Slowing down as an early warning signal for abrupt climate change. Proc. Natl. Acad. Sci. Unit. States Am. 105, 14308–14312.

Dansgaard, W., Johnsen, S.J., Clausen, H.B., Dahl-Jensen, D., Gundestrup, N.S., Hammer, C.U., Hvidberg, C.S., Steffensen, J.P., Sveinbjörnsdottir, A.E., Jouzel, J., Bond, G., 1993. Evidence for general instability of past climate from a 250-kyr ice-core record. Nature 364, 218–220. https://doi.org/10.1038/364218a0.

deMenocal, P.B., 1995. Plio-pleistocene african climate. Science 270, 53–59. https://doi.org/10.1126/science.270.5233.53.

DeMenocal, P.B., 2004. African climate change and faunal evolution during the Pliocene–Pleistocene. Earth Planet Sci. Lett. 220, 3–24. https://doi.org/10.1016/S0012-821X(04)00003-2.

Donges, J.F., Donner, R.V., Kurths, J., 2013. Testing time series irreversibility using complex network methods. EPL (Europhysics Letters) 102, 10004. https://doi.org/10.1209/0295-5075/102/10004.

Donges, J.F., Donner, R.V., Marwan, N., Breitenbach, S.F.M., Rehfeld, K., Kurths, J., 2015a. Non-linear regime shifts in Holocene Asian monsoon variability: potential impacts on cultural change and migratory patterns. Clim. Past 11, 709–741. https://doi.org/10.5194/cp-11-709-2015.

Donges, J.F., Donner, R.V., Rehfeld, K., Marwan, N., Trauth, M.H., Kurths, J., 2011a. Identification of dynamical transitions in marine palaeoclimate records by recurrence network analysis. Nonlinear Process Geophys. 18, 545–562. https://doi.org/10.5194/npg-18-545-2011.

Donges, J.F., Donner, R.V., Trauth, M.H., Marwan, N., Schellnhuber, H.J., Kurths, J., 2011b. Nonlinear detection of paleoclimate-variability transitions possibly related to human evolution. Proc. Natl. Acad. Sci. Unit. States Am. 108, 20422–20427. https://doi.org/10.1073/pnas.1117052108.

Donges, J.F., Heitzig, J., Beronov, B., Wiedermann, M., Runge, J., Feng, Q.Y., Tupikina, L., Stolbova, V., Donner, R.V., Marwan, N., Dijkstra, H.A., Kurths, J., 2015b. Unified functional network and nonlinear time series analysis for complex systems science: the pyunicorn package. Chaos 25, 113101. https://doi.org/10.1063/1.4934554.

Donner, R.V., Heitzig, J., Donges, J.F., Zou, Y., Marwan, N., Kurths, J., 2011. The geometry of chaotic dynamics – a complex network perspective. Euro. Phys. J. B 84, 653–672. https://doi.org/10.1140/epjb/e2011-10899-1.

Donner, R.V., Zou, Y., Donges, J.F., Marwan, N., Kurths, J., 2010. Recurrence networks – a novel paradigm for nonlinear time series analysis. New J. Phys. 12, 033025. https://doi.org/10.1088/1367-2630/12/3/033025.

Eckmann, J.P., Ruelle, D., 1992. Fundamental limitations for estimating dimensions and Lyapunov exponents in dynamical systems. Physica D 56, 185–187. https://doi.org/10.1016/0167-2789(92)90023-G.

Eroglu, D., McRobie, F.H., Ozken, I., Stemler, T., Wyrwoll, K.H., Breitenbach, S.F.M., Marwan, N., Kurths, J., 2016. See-saw relationship of the Holocene East Asian-Australian summer monsoon. Nat. Commun. 7, 12929. https://doi.org/10.1038/ncomms12929.

Fan, J., Meng, J., Ludescher, J., Chen, X., Ashkenazy, Y., Kurths, J., Havlin, S., Schellnhuber, H.J., 2021. Statistical physics approaches to the complex Earth system. Phys. Rep. 896, 1–84. https://doi.org/10.1016/j.physrep.2020.09.005.

Feldhoff, J.H., Donner, R.V., Donges, J.F., Marwan, N., Kurths, J., 2012. Geometric detection of coupling directions by means of inter-system recurrence networks. Phys. Lett. 376, 3504–3513. https://doi.org/10.1016/j.physleta.2012.10.008.

Friedrich, R., Peinke, J., Sahimi, M., Reza Rahimi Tabar, M., 2011. Approaching complexity by stochastic methods: from biological systems to turbulence. Phys. Rep. 506, 87–162. https://doi.org/10.1016/j.physrep.2011.05.003.

Gao, Z.K., Cai, Q., Yang, Y.X., Dang, W.D., Zhang, S.S., 2016. Multiscale limited penetrable horizontal visibility graph for analyzing nonlinear time series. Sci. Rep. 6, 35622. https://doi.org/10.1038/srep35622.

Gapelyuk, A., Schirdewan, A., Fischer, R., Wessel, N., 2010. Cardiac magnetic field mapping quantified by Kullback–Leibler entropy detects patients with coronary artery disease. Physiol. Meas. 31, 1345–1354. https://doi.org/10.1088/0967-3334/31/10/004.

Gardiner, C., 2009. Stochastic Methods – A Handbook for the Natural and Social Sciences. Springer Berlin Heidelberg, Berlin, Heidelberg.

Garland, J., Jones, T., Neuder, M., Morris, V., White, J., Bradley, E., 2018. Anomaly detection in paleoclimate records using permutation entropy. Entropy 20, 931. https://doi.org/10.3390/e20120931.

Gershenfeld, N.A., 1992. Dimension measurement on high-dimensional systems. Phys. Nonlinear Phenom. 55, 135–154. https://doi.org/10.1016/0167-2789(92)90193-Q.

Ghil, M., 2002. Advanced spectral methods for climatic time series. Rev. Geophys. 40, 1003. https://doi.org/10.1029/2000RG000092.

Goswami, B., Boers, N., Rheinwalt, A., Marwan, N., Heitzig, J., Breitenbach, S.F.M., Kurths, J., 2018. Abrupt transitions in time series with uncertainties. Nat. Commun. 9, 48. https://doi.org/10.1038/s41467-017-02456-6.

Goswami, B., Marwan, N., Feulner, G., Kurths, J., 2013. How do global temperature drivers influence each other? – a network perspective using recurrences. Eur. Phys. J. Spec. Top. 222, 861–873. https://doi.org/10.1140/epjst/e2013-01889-8.

Grassberger, P., 1986. Do climatic attractors exist? Nature 323, 609–612. https://doi.org/10.1038/323609a0.

Grassberger, P., Procaccia, I., 1983. Measuring the strangeness of strange attractors. Physica D 9, 189–208. https://doi.org/10.1016/0167-2789(83)90298-1.

Grassberger, P., Procaccia, I., 1984. Dimensions and entropies of strange attractors from a fluctuating dynamics approach. Phys. Lett. 13, 34–54. https://doi.org/10.1016/0167-2789(84)90269-0.

Han, W., Appel, E., Galy, A., Rösler, W., Fang, X., Zhu, X., Vandenberghe, J., Wang, J., Berger, A., Lü, S., Zhang, T., 2020. Climate transition in the Asia inland at 0.8–0.6

Ma related to astronomically forced ice sheet expansion. Quat. Sci. Rev. 248, 106580. https://doi.org/10.1016/j.quascirev.2020.106580.
Hannisdal, B., 2011. Non-parametric inference of causal interactions from geological records. Am. J. Sci. 311, 315–334. https://doi.org/10.2475/04.2011.02.
Hassanibesheli, F., Boers, N., Kurths, J., 2020. Reconstructing complex system dynamics from time series: a method comparison. New J. Phys. 22, 073053. https://doi.org/10.1088/1367-2630/ab9ce5.
Haug, G.H., Tiedemann, R., 1998. Effect of the formation of the isthmus of Panama on Atlantic ocean thermohaline circulation. Nature 393, 673–676. https://doi.org/10.1038/31447.
Herbert, T.D., Peterson, L.C., Lawrence, K.T., Liu, Z., 2010. Tropical ocean temperatures over the past 3.5 million years. Science 328, 1530–1534. https://doi.org/10.1126/science.1185435.
Hughes, T.P., Carpenter, S., Rockström, J., Scheffer, M., Walker, B., 2013. Multiscale regime shifts and planetary boundaries. Trends Ecol. Evol. 28, 389–395.
Kantz, H., 1994. Quantifying the closeness of fractal measures. Phys. Rev. 49, 5091–5097. https://doi.org/10.1103/PhysRevE.49.5091.
Kantz, H., Schreiber, T., 1997. Nonlinear Time Series Analysis. University Press, Cambridge.
Kennel, M.B., Brown, R., Abarbanel, H.D.I., 1992. Determining embedding dimension for phase-space reconstruction using a geometrical construction. Phys. Rev. 45, 3403–3411. https://doi.org/10.1103/PhysRevA.45.3403.
Kraemer, K.H., Datseris, G., Kurths, J., Kiss, I.Z., Ocampo-Espindola, J.L., Marwan, N., 2021. A unified and automated approach to attractor reconstruction. New J. Phys. 23, 033017. https://doi.org/10.1088/1367-2630/abe336.
Kraemer, K.H., Donner, R.V., Heitzig, J., Marwan, N., 2018. Recurrence threshold selection for obtaining robust recurrence characteristics in different embedding dimensions. Chaos 28, 085720. https://doi.org/10.1063/1.5024914.
Kwasniok, F., Lohmann, G., 2009. Deriving dynamical models from paleoclimatic records: application to glacial millennial-scale climate variability. Phys. Rev. 80, 1–9. https://doi.org/10.1103/PhysRevE.80.066104.
Kwasniok, F., Lohmann, G., 2012. A stochastic nonlinear oscillator model for glacial millennial-scale climate transitions derived from ice-core data. Nonlinear Process Geophys. 19, 595–603. https://doi.org/10.5194/npg-19-595-2012.
Lacasa, L., Luque, B., Ballesteros, F., Luque, J., Nuño, J.C., 2008. From time series to complex networks: the visibility graph. Proc. Natl. Acad. Sci. Unit. States Am. 105, 4972. https://doi.org/10.1073/pnas.0709247105.
Lacasa, L., Luque, B., Luque, J., Nuño, J.C., 2009. The visibility graph: a new method for estimating the Hurst exponent of fractional Brownian motion. EPL (Europhysics Letters) 86, 30001. https://doi.org/10.1209/0295-5075/86/30001.
Lacasa, L., Nuñez, A., Roldán, É., Parrondo, J.M.R., Luque, B., 2012. Time series irreversibility: a visibility graph approach. Eur. Phys. J. B 85, 217. https://doi.org/10.1140/epjb/e2012-20809-8.
Larrasoaña, J.C., Roberts, A.P., Rohling, E.J., Winklhofer, M., Wehausen, R., 2003. Three million years of monsoon variability over the northern Sahara. Clim. Dynam. 21, 689–698. https://doi.org/10.1007/s00382-003-0355-z.
Lawrance, A.J., 1991. Directionality and reversibility in time series. Int. Stat. Rev./Rev. Int. Stat. 59, 67. https://doi.org/10.2307/1403575.
Lechleitner, F.A., Breitenbach, S.F.M., Cheng, H., Plessen, B., Rehfeld, K., Goswami, B., Marwan, N., Eroglu, D., Adkins, J., Haug, G., 2017. Climatic and in-cave influences on δ^{18}O and δ^{13}C in a stalagmite from northeastern India through the last deglaciation. Quat. Res. 88, 458–471. https://doi.org/10.1017/qua.2017.72.
Lekscha, J., Donner, R., 2020. Detecting dynamical anomalies in time series from different palaeoclimate proxy archives using windowed recurrence network analysis. Nonlinear Process Geophys. 27, 261–275. https://doi.org/10.5194/npg-27-261-2020.
Lekscha, J., Donner, R.V., 2018. Phase space reconstruction for non-uniformly sampled noisy time series. Chaos 28, 085702. https://doi.org/10.1063/1.5023860.
Lenton, T.M., Held, H., Kriegler, E., Hall, J.W., Lucht, W., Rahmstorf, S., Schellnhuber, H.J., 2008. Tipping elements in the earth's climate system. Proc. Natl. Acad. Sci. Unit. States Am. 105, 1786–1793.
Li, W.L., Zhong, W.Q., Jin, B.S., Xiao, R., He, T.T., 2013. Flow regime identification in a three-phase bubble column based on statistical, Hurst, Hilbert–Huang transform and Shannon entropy analysis. Chem. Eng. Sci. 102, 474–485. https://doi.org/10.1016/j.ces.2013.08.052.
Lisiecki, L.E., 2010. Links between eccentricity forcing and the 100,000-year glacial cycle. Nat. Geosci. 3, 349–352. https://doi.org/10.1038/ngeo828.
Lisiecki, L.E., Raymo, M.E., 2005. A Pliocene-Pleistocene stack of 57 globally distributed benthic δ 18O records. Paleoceanography 20, 1–17. https://doi.org/10.1029/2004PA001071.
Little, M.A., McSharry, P.E., Roberts, S.J., Costello, D.A.E., Moroz, I.M., 2007. Exploiting nonlinear recurrence and fractal scaling properties for voice disorder detection. Biomed. Eng. Online 6, 1–19. https://doi.org/10.1186/1475-925X-6-23.
Livina, V., Ditlevsen, P., Lenton, T., 2012. An independent test of methods of detecting system states and bifurcations in time-series data. Phys. Stat. Mech. Appl. 391, 485–496. https://doi.org/10.1016/j.physa.2011.08.025.
Livina, V.N., Kwasniok, F., Lenton, T.M., 2010. Potential analysis reveals changing number of climate states during the last 60 kyr. Clim. Past 6, 77–82. https://doi.org/10.5194/cp-6-77-2010.
Livina, V.N., Kwasniok, F., Lohmann, G., Kantelhardt, J.W., Lenton, T.M., 2011. Changing climate states and stability: from Pliocene to present. Clim. Dynam. 37, 2437–2453. https://doi.org/10.1007/s00382-010-0980-2.
Lourens, L.J., Antonarakou, A., Hilgen, F.J., Van Hoof, A.A.M., Vergnaud-Grazzini, C., Zachariasse, W.J., 1996. Evaluation of the Plio-Pleistocene astronomical timescale. Paleoceanography 11, 391–413. https://doi.org/10.1029/96PA01125.
Maasch, K.A., 1989. Calculating climate attractor dimension from δ18O records by the Grassberger-Procaccia algorithm. Clim. Dynam. 4, 45–55. https://doi.org/10.1007/BF00207399.
Malik, N., Marwan, N., Zou, Y., Mucha, P.J., Kurths, J., 2014. Fluctuation of similarity to detect transitions between distinct dynamical regimes in short time series. Phys. Rev. 89, 062908. https://doi.org/10.1103/PhysRevE.89.062908.
Marwan, N., 2008. A historical review of recurrence plots. Eur. Phys. J. Spec. Top. 164, 3–12. https://doi.org/10.1140/epjst/e2008-00829-1.
Marwan, N., 2011. How to avoid potential pitfalls in recurrence plot based data analysis. Int. J. Bifurcation Chaos 21, 1003–1017. https://doi.org/10.1142/S0218127411029008.
Marwan, N., Donges, J.F., Zou, Y., Donner, R.V., Kurths, J., 2009. Complex network approach for recurrence analysis of time series. Phys. Lett. 373, 4246–4254. https://doi.org/10.1016/j.physleta.2009.09.042.
Marwan, N., Kurths, J., 2015. Complex network based techniques to identify extreme events and (sudden) transitions in spatio-temporal systems. Chaos 25, 097609. https://doi.org/10.1063/1.4916924.
Marwan, N., Romano, M.C., Thiel, M., Kurths, J., 2007. Recurrence plots for the analysis of complex systems. Phys. Rep. 438, 237–329. https://doi.org/10.1016/j.physrep.2006.11.001.
Marwan, N., Schinkel, S., Kurths, J., 2013. Recurrence plots 25 years later – gaining confidence in dynamical transitions. Europhys. Lett. 101, 20007. https://doi.org/10.1209/0295-5075/101/20007.
Marwan, N., Trauth, M.H., Vuille, M., Kurths, J., 2003. Comparing modern and Pleistocene ENSO-like influences in NW Argentina using nonlinear time series analysis methods. Clim. Dynam. 21, 317–326. https://doi.org/10.1007/s00382-003-0335-3.
Marwan, N., Wessel, N., Meyerfeldt, U., Schirdewan, A., Kurths, J., 2002. Recurrence plot based measures of complexity and its application to heart rate variability data. Phys. Rev. 66, 026702. https://doi.org/10.1103/PhysRevE.66.026702.
Möller, M., Lange, W., Mitschke, F., Abraham, N., Hübner, U., 1989. Errors from digitizing and noise in estimating attractor dimensions. Phys. Lett. 138, 176–182. https://doi.org/10.1016/0375-9601(89)90023-6.
Mudelsee, M., Schulz, M., 1997. The Mid-Pleistocene climate transition: onset of 100 ka cycle lags ice volume build-up by 280 ka. Earth Planet Sci. Lett. 151, 117–123. https://doi.org/10.1016/S0012-821X(97)00114-3.
Mudelsee, M., Stattegger, K., 1997. Exploring the structure of the mid-Pleistocene revolution with advanced methods of time-series analysis. Geol. Rundsch. 86, 499–511. https://doi.org/10.1007/s005310050157.
Ozken, I., Eroglu, D., Stemler, T., Marwan, N., Bagci, G.B., Kurths, J., 2015. Transformation-cost time-series method for analyzing irregularly sampled data. Phys. Rev. 91, 062911. https://doi.org/10.1103/PhysRevE.91.062911.
Packard, N.H., Crutchfield, J.P., Farmer, J.D., Shaw, R.S., 1980. Geometry from a time series. Phys. Rev. Lett. 45, 712–716. https://doi.org/10.1103/PhysRevLett.45.712.
Pessa, A.A.B., Ribeiro, H.V., 2021. ordpy: a Python package for data analysis with permutation entropy and ordinal network methods. Chaos 31, 063110. https://doi.org/10.1063/5.0049901.
Petrick, B., Martínez-García, A., Auer, G., Reuning, L., Auderset, A., Deik, H., Takayanagi, H., De Vleeschouwer, D., Iryu, Y., Haug, G.H., 2019. Glacial Indonesian throughflow weakening across the mid-pleistocene climatic transition. Sci. Rep. 9, 16995. https://doi.org/10.1038/s41598-019-53382-0.
Potts, R., 1996. Evolution and climate variability. Science 273, 922–923. https://doi.org/10.1126/science.273.5277.922.
Prasad, S., Marwan, N., Eroglu, D., Goswami, B., Mishra, P.K., Gaye, B., Anoop, A., Basavaiah, N., Stebich, M., Jehangir, A., 2020. Holocene climate forcings and lacustrine regime shifts in the Indian summer monsoon realm. Earth Surf. Process. Landforms 45, 3842–3853. https://doi.org/10.1002/esp.5004.
Ravelo, A.C., Andreasen, D.H., Lyle, M., Olivarez Lyle, A., Wara, M.W., 2004. Regional climate shifts caused by gradual global cooling in the Pliocene epoch. Nature 429, 263–267. https://doi.org/10.1038/nature02567.
Rawald, T., Sips, M., Marwan, N., 2017. PyRQA – conducting recurrence quantification analysis on very long time series efficiently. Comput. Geosci. 104, 101–108. https://doi.org/10.1016/j.cageo.2016.11.016.
Rehfeld, K., Marwan, N., Breitenbach, S.F.M., Kurths, J., 2013. Late Holocene Asian summer monsoon dynamics from small but complex networks of paleoclimate data. Clim. Dynam. 41, 3–19. https://doi.org/10.1007/s00382-012-1448-3.
Rehfeld, K., Marwan, N., Heitzig, J., Kurths, J., 2011. Comparison of correlation analysis techniques for irregularly sampled time series. Nonlinear Process Geophys. 18, 389–404. https://doi.org/10.5194/npg-18-389-2011.
Richman, J.S., Moorman, J.R., 2000. Physiological time-series analysis using approximate entropy and sample entropy. Am. J. Physiol. Heart Circ. Physiol. 278, H2039–H2049.
Risken, H., 1989. The Fokker-Planck Equation. Volume 18 *of Springer Series in Synergetics*. Springer Berlin Heidelberg, Berlin, Heidelberg. https://doi.org/10.1007/978-3-642-61544-3.
Rocha, J.C., Peterson, G., Bodin, Ö., Levin, S., 2018. Cascading regime shifts within and across scales. Science 362, 1379–1383.
Rockström, J., Steffen, W., Noone, K., Persson, Å., Chapin, F.S., Lambin, E.F., Lenton, T.M., Scheffer, M., Folke, C., Schellnhuber, H.J., et al., 2009. A safe operating space for humanity. nature 461, 472–475.
Rosenstein, M.T., Collins, J.J., De Luca, C.J., 1993. A practical method for calculating largest Lyapunov exponents from small data sets. Phys. Nonlinear Phenom. 65, 117–134. https://doi.org/10.1016/0167-2789(93)90009-P.
Sauramo, M., 1918. Geochronologische studien über die spätglaziale zeit in

südfinnland. Bull. Comm. Geol. Finl. 50, 3–48.
Scheffer, M., Bascompte, J., Brock, W.A., Brovkin, V., Carpenter, S.R., Dakos, V., Held, H., Van Nes, E.H., Rietkerk, M., Sugihara, G., 2009. Early-warning signals for critical transitions. Nature 461, 53–59.
Scheffer, M., Carpenter, S.R., 2003. Catastrophic regime shifts in ecosystems: linking theory to observation. Trends Ecol. Evol. 18, 648–656.
Schellnhuber, H.J., 2009. Tipping elements in the earth system. Proc. Natl. Acad. Sci. Unit. States Am. 106, 20561–20563.
Schleussner, C.F., Divine, D.V., Donges, J.F., Miettinen, A., Donner, R.V., 2015. Indications for a North Atlantic ocean circulation regime shift at the onset of the Little ice Age. Clim. Dynam. 45, 3623–3633. https://doi.org/10.1007/s00382-015-2561-x.
Schölzel, C., Friederichs, P., 2008. Multivariate non-normally distributed random variables in climate research – introduction to the copula approach. Nonlinear Process Geophys. 15, 761–772. https://doi.org/10.5194/npg-15-761-2008.
Schulz, M., Mudelsee, M., Wolf-Welling, T., 1994. Fractal analyses of pleistocene marine oxygen isotope records. In: Fractals and Dynamic Systems in Geoscience. Springer, Berlin Heidelberg, pp. 377–387.
Schütz, N., Holschneider, M., 2011. Detection of trend changes in time series using Bayesian inference. Phys. Rev. 84, 021120. https://doi.org/10.1103/PhysRevE.84.021120.
Shannon, C., 1948. A mathematical theory of communication. Bell System Technical Journal, The 27, 379–423. https://doi.org/10.1002/j.1538-7305.1948.tb01338.x.
Silverman, B.W., 1986. Density Estimation for Statistics and Data Analysis, vol. 26. CRC Press.
Singh, M., Krishnan, R., Goswami, B., Choudhury, A.D., Swapna, P., Vellore, R., Prajeesh, A.G., Sandeep, N., Venkataraman, C., Donner, R.V., Marwan, N., Kurths, J., 2020. Fingerprint of volcanic forcing on the ENSO–Indian monsoon coupling. Sci. Adv. 6, eaba8164. https://doi.org/10.1126/sciadv.aba8164.
Smirnov, D.A., Marwan, N., Breitenbach, S.F.M., Lechleitner, F., Kurths, J., 2017. Coping with dating errors in causality estimation. Europhys. Lett. 117, 10004. https://doi.org/10.1209/0295-5075/117/10004.
Spiridonov, A., Balakauskas, L., Stankevic, R., Kluczynska, G., Gedminiene, L., Stancikaite, M., 2019. Holocene vegetation patterns in southern Lithuania indicate astronomical forcing on the millennial and centennial time scales. Sci. Rep. 9, 14711. https://doi.org/10.1038/s41598-019-51321-7.
Spiridonov, A., Stankevič, R., Gečas, T., Brazauskas, A., Kaminskas, D., Musteikis, P., Kaveckas, T., Meidla, T., Bičkauskas, G., Ainsaar, L., Radzevičius, S., 2020. Ultra-high resolution multivariate record and multiscale causal analysis of Pridoli (late Silurian): implications for global stratigraphy, turnover events, and climate-biota interactions. Gondwana Res. 86, 222–249. https://doi.org/10.1016/j.gr.2020.05.015.
Spiridonov, A., Vaikutienė, G., Stankevič, R., Druzhinina, O., Šeirienė, V., Subetto, D., Kublitsky, J., Stančikaitė, M., 2021. Response of freshwater diatoms to cold events in the late pleistocene and early Holocene (SE Baltic region). Quat. Int. 589, 112–123. https://doi.org/10.1016/j.quaint.2021.02.017.
Stanley, D.J., 1978. Ionian Sea sapropel distribution and late Quaternary palaeoceanography in the eastern Mediterranean. Nature 274, 149.
Staubwasser, M., Weiss, H., 2006. Holocene climate and cultural evolution in late prehistoric–early historic West Asia. Quat. Res. 66, 372–387. https://doi.org/10.1016/j.yqres.2006.09.001.
Steffen, W., Richardson, K., Rockström, J., Cornell, S.E., Fetzer, I., Bennett, E.M., Biggs, R., Carpenter, S.R., De Vries, W., De Wit, C.A., et al., 2015. Planetary boundaries: guiding human development on a changing planet. Science 347.
Steffen, W., Rockström, J., Richardson, K., Lenton, T.M., Folke, C., Liverman, D., Summerhayes, C.P., Barnosky, A.D., Cornell, S.E., Crucifix, M., et al., 2018. Trajectories of the earth system in the anthropocene. Proc. Natl. Acad. Sci. Unit. States Am. 115, 8252–8259.
Supriya, S., Siuly, S., Wang, H., Cao, J., Zhang, Y., 2016. Weighted visibility graph with complex network features in the detection of epilepsy. IEEE Access 4, 6554–6566. https://doi.org/10.1109/ACCESS.2016.2612242.
Takens, F., 1981. Detecting strange attractors in turbulence. In: Rand, D., Young, L.S. (Eds.), Dynamical Systems and Turbulence. Springer, Berlin, pp. 366–381 volume 898 *of Lecture Notes in Mathematics*.
Theiler, J., Eubank, S., Longtin, A., Galdrikian, B., Farmer, B., 1992. Testing for nonlinearity in time series: the method of surrogate data. Physica D 58, 77–94. https://doi.org/10.1016/0167-2789(92)90102-S.
Thiel, M., Romano, M.C., Read, P.L., Kurths, J., 2004. Estimation of dynamical invariants without embedding by recurrence plots. Chaos 14, 234–243. https://doi.org/10.1063/1.1667633.
Tiedemann, R., Sarnthein, M., Shackleton, N.J., 1994. Astronomic timescale for the Pliocene Atlantic $\delta^{18}O$ and dust flux records of ocean drilling program site 659. Paleoceanography 9, 619–638.
Trauth, M.H., 2005. Late cenozoic moisture history of east Africa. Science 309, 2051–2053. https://doi.org/10.1126/science.1112964.
Trauth, M.H., 2021. Spectral analysis in quaternary sciences. Quat. Sci. Rev. 270, 107157. https://doi.org/10.1016/j.quascirev.2021.107157.
Trauth, M.H., Asrat, A., Cohen, A.S., Duesing, W., Foerster, V., Kaboth-Bahr, S., Kraemer, K.H., Lamb, H.F., Marwan, N., Maslin, M.A., Schäbitz, F., 2021. Recurring types of variability and transitions in the ~ 620 kyr record of climate change from the Chew Bahir basin, southern Ethiopia. Quat. Sci. Rev. 266, 106777. https://doi.org/10.1016/j.quascirev.2020.106777.
Trauth, M.H., Larrasoña, J.C., Mudelsee, M., 2009. Trends, rhythms and events in plio-pleistocene african climate. Quat. Sci. Rev. 28, 399–411. https://doi.org/10.1016/j.quascirev.2008.11.003.
Vautard, R., Ghil, M., 1989. Singular spectrum analysis in nonlinear dynamics, with applications to paleoclimatic time series. Phys. Nonlinear Phenom. 35, 395–424. https://doi.org/10.1016/0167-2789(89)90077-8.
Voss, H., Kurths, J., Schwarz, U., 1996. Reconstruction of grand minima of solar activity from radiocarbon data. J. Geophys. Res. 101, 15637–15643. https://doi.org/10.1029/96JA00542.
Webber Jr., C.L., Marwan, N., Facchini, A., Giuliani, A., 2009. Simpler methods do it better: success of Recurrence Quantification Analysis as a general purpose data analysis tool. Phys. Lett. 373, 3753–3756. https://doi.org/10.1016/j.physleta.2009.08.052.
Westerhold, T., Marwan, N., Drury, A.J., Liebrand, D., Agnini, C., Anagnostou, E., Barnet, J.S.K., Bohaty, S.M., De Vleeschouwer, D., Florindo, F., Frederichs, T., Hodell, D.A., Holbourn, A.E., Kroon, D., Lauretano, V., Littler, K., Lourens, L.J., Lyle, M., Pälike, H., Röhl, U., Tian, J., Wilkens, R.H., Wilson, P.A., Zachos, J.C., 2020. An astronomically dated record of Earth's climate and its predictability over the last 66 million years. Science 369, 1383–1387. https://doi.org/10.1126/science.aba6853.
Wolf, A., Swift, J.B., Swinney, H.L., Vastano, J.A., 1985. Determining Lyapunov exponents from a time series. Physica D 16, 285–317. https://doi.org/10.1016/0167-2789(85)90011-9.
Zanin, M., Olivares, F., 2021. Ordinal patterns-based methodologies for distinguishing chaos from noise in discrete time series. Commun. Phys. 4, 190. https://doi.org/10.1038/s42005-021-00696-z.
Zbilut, J.P., Webber Jr., C.L., 2007. Recurrence quantification analysis: introduction and historical context. Int. J. Bifurcation Chaos 17, 3477–3481. https://doi.org/10.1142/S0218127407019238.
Zhao, X., Ji, M., Zhang, N., Shang, P., 2020. Permutation transition entropy: measuring the dynamical complexity of financial time series. Chaos, Solit. Fractals 139, 109962. https://doi.org/10.1016/j.chaos.2020.109962.
Zou, Y., Donner, R., Marwan, N., Small, M., Kurths, J., 2014. Long-term changes in the north-south asymmetry of solar activity: a nonlinear dynamics characterization using visibility graphs. Nonlinear Process Geophys. 21. https://doi.org/10.5194/npg-21-1113-2014.
Zou, Y., Donner, R.V., Donges, J.F., Marwan, N., Kurths, J., 2010. Identifying complex periodic windows in continuous-time dynamical systems using recurrence-based methods. Chaos 20, 043130. https://doi.org/10.1063/1.3523304.
Zou, Y., Donner, R.V., Marwan, N., Donges, J.F., Kurths, J., 2019. Complex network approaches to nonlinear time series analysis. Phys. Rep. 787, 1–97. https://doi.org/10.1016/j.physrep.2018.10.005.